

Wind Structure Discrepancies between Two Best Track Datasets for Western North Pacific Tropical Cyclones

JINJIE SONG

Key Laboratory of Mesoscale Severe Weather, Ministry of Education, and School of Atmospheric Sciences, Nanjing University, and Joint Center for Atmospheric Radar Research of Centre of Modern Analysis/Nanjing University (CMA/NJU), Nanjing, China

PHILIP J. KLOTZBACH

Department of Atmospheric Science, Colorado State University, Fort Collins, Colorado

(Manuscript received 2 May 2016, in final form 3 August 2016)


ABSTRACT

Symmetric and wavenumber-1 asymmetric characteristics of western North Pacific tropical cyclone (TC) outer wind structures are compared between best tracks from the Joint Typhoon Warning Center (JTWC) and the Japan Meteorological Agency (JMA) from 2004 to 2014 as well as the Multiplatform Tropical Cyclone Surface Wind Analysis (MTCSWA) product from 2007 to 2014. Significant linear relationships of averaged wind radii are obtained among datasets, in which both gale-force and storm-force wind radii are generally estimated slightly smaller (much larger) by JTWC (JMA) than by MTCSWA. These correlations are strongly related to TC intensity relationships discussed in earlier work. Moreover, JTWC (JMA) on average represents a smaller (greater) derived shape parameter than MTCSWA does, implying that JTWC (JMA) typically assesses a more compact (less compact) storm than MTCSWA. For the wavenumber-1 asymmetry, large differences among datasets are found regardless of the magnitude or the direction of the longest radius. JTWC estimates more asymmetric storms than JMA, and it provides greater wavenumber-1 asymmetry magnitudes on average. Asymmetric storms are most frequently oriented toward the east, northeast, and north in JTWC and MTCSWA, whereas they are most frequently oriented toward the southeast, east, and northeast in JMA. The direction of the longest gale-force (storm force) wind radius in JTWC is statistically rotated 18° (32°) clockwise to that in JMA. Although the wind radii in JTWC are of higher quality than those in JMA when using MTCSWA as a baseline, there remains a need to provide a consistent and reliable wind radii estimating process among operational centers.

1. Introduction

Tropical cyclones (TCs) are one of the most violent natural disasters over the western North Pacific (WNP), often causing severe economic and human losses in the coastal regions of East and Southeast Asian countries. While maximum sustained wind (VMAX) is most related to the potential damage of a given TC near the region of strongest winds, it is the storm structure that is

the best parameter for estimating the total impact of the TC (Knaff 2006). The damage potential of a storm is directly related to its intensity, which is defined in terms of the VMAX at 10 m over a time averaging period (Landsea 1993). This quantity has been long estimated by aircraft reconnaissance and satellite surveillance in many operational TC forecasting centers (Velden et al. 2006). To facilitate data retrieval, the intensity of a storm has been recorded at 6-h intervals in so-called best track datasets (BTDs). Many operational agencies have provided their own BTDs of WNP TCs, which are now archived in the International Best Track Archive for Climate Stewardship (IBTrACS) (Knapp et al. 2010). Agencies providing BTDs for WNP TCs include the U.S. Department of Defense Joint Typhoon Warning Center (JTWC), the Japan Meteorological

 Denotes Open Access content.

Corresponding author address: Jinjie Song, 163 Xianlin Rd., Nanjing 210023, China.
E-mail: songjinjie@nju.edu.cn

DOI: 10.1175/MWR-D-16-0163.1

© 2016 American Meteorological Society

Agency (JMA), the China Meteorological Administration's Shanghai Typhoon Institute (CMA/STI), and the Hong Kong Observatory (HKO). However, significant discrepancies of estimated VMAX have been found among different BTDs in many previous publications (e.g. Wu et al. 2006; Yeung 2006; Kamahori et al. 2006; Yu et al. 2007; Nakazawa and Hoshino 2009; Song et al. 2010; Knapp and Kruk 2010; Ren et al. 2011; Barcikowska et al. 2012; Kang and Elsner 2012). It has been found that these inconsistent VMAX diagnostics are at least the result of two factors. One is the use of different averaging periods for calculating VMAX, and the other is the different procedures in which VMAX is estimated from various observational platforms and retrieval algorithms (Kang and Elsner 2012). There has yet to be a consensus among the research community as to which BTD is the most reliable (Kang and Elsner 2016).

There are several quantities that describe the storm structure near the surface, including the radius of maximum wind (RMW), the eye diameter, the radius of the outermost closed isobar (ROCI), and the size of the wind field. These structural metrics can be estimated based on surface winds retrieved from various satellite and costal radar products (Chu et al. 2002). Compared with other structural metrics, the size of the wind field is vital in determining storm-related impacts such as areas impacted by destructive winds and storm surges (Knaff 2006). Because of the difficulty in observing and verifying wind fields associated with TCs, only two operational agencies, JTWC and JMA, provide TC wind field information over the WNP in their BTDs. The radii of specified winds (e.g. 30, 34, 50 kt, etc.; $1 \text{ kt} = 0.5144 \text{ m s}^{-1}$) are recorded every 6 h in the JTWC and JMA BTDs. These wind radii are subjectively estimated by operational forecasters using all of the available observational products at that time. The real-time estimated wind radii are directly recorded in the JTWC BTD without a postanalysis. In contrast, these wind radii are reviewed and updated postanalysis by JMA before being included in its BTD. Despite different processes in deriving BTDs, both wind radii for JTWC and JMA are often considered as the best estimates of the "true" values. As a result, wind radii of WNP TCs provided in both BTDs have been widely used to investigate climatological characteristics of TC wind structure (Lei and Chen 2005; Yuan et al. 2007a,b; Lu et al. 2011), to develop and verify objective techniques of estimating TC size (Lee et al. 2010; Cheung et al. 2011), and to build operational prediction models of TC wind fields and their related impacts (Knaff et al. 2007; Sampson et al. 2010).

As Song et al. (2010) have pointed out, inconsistent VMAX records from several BTDs lead to different

estimated long-term trends of WNP TC potential destructiveness. Nonetheless, it is still unknown whether the recorded wind radii are consistent between the JTWC and JMA BTDs. If there are significant differences in wind radii between the two BTDs, this would explain several conflicting findings and conclusions given in previous papers. For example, Lu et al. (2011) analyzed the JTWC estimated wind radii from 2001 to 2006. The average TC size in their paper was 203 km. However, the mean TC size was reported to be 350 km in Yuan et al. (2007b) when the JMA BTD was used between 1977 and 2004. Furthermore, Cheung et al. (2011) obtained the mean radii of 50-kt winds (R_{50}) in four quadrants (viz., northeast, southeast, southwest, and northwest) derived from the JTWC and JMA BTDs from 2006 to 2009. The quadrant average of $R_{50, \text{JTWC}}$ was 14% (around 15 km) smaller than that of $R_{50, \text{JMA}}$. Although the wind radii provided by JTWC are generally smaller than those estimated by JMA, the quantitative relationship between the two BTDs is still unclear. It is thus one goal of our work to investigate the quantitative relationship of the mean wind radii (symmetric structure) for those storms that were simultaneously recorded by JTWC and JMA (hereafter concurrent TCs). Beyond that, it is also examined in this study whether the asymmetric structures of wind fields are correlated between the two BTDs. Another aspect of this study is evaluating the qualities of wind fields estimated in two BTDs by using a control dataset (e.g. a satellite-based TC surface wind field product). It is investigated in this work whether the TC size estimates in one BTD are superior to that in the other BTD.

This article is organized as follows. Section 2 describes the wind radii data used in this study and the method of decomposing the wind field into its symmetric and asymmetric structures. Section 3 discusses the statistical links between storm wind radii and other TC metrics among BTDs and the satellite-based product. Section 4 examines the wind fields' potential differences and their quantitative relationship among datasets. The final section presents a summary of this work.

2. Wind radius data and their decompositions

The information on the TC wind fields used here are from the JTWC and JMA BTDs of 6-hourly storm observations. Because of the lack of in situ observations, the estimation of TC wind radii relies very heavily on satellites, particularly scatterometers, by both agencies. JTWC primarily uses scatterometer products to estimate TC wind structure in their operations. These analyzed wind radii are directly recorded in the JTWC BTD without quality control (B. Strahl 2016, personal

communication). JMA also operationally applies scatterometers to analyze the TC wind structure. The Quick Scatterometer (QuikSCAT) and Advanced Scatterometer (ASCAT) sea surface wind data are used as reference in determining TC wind radii before and after 2007, respectively (Kunitsugu 2012; H. Ishihara 2016, personal communication). The analyzed wind radii are then reviewed and updated with delayed information (e.g. ship/SYNOP reports) before they are listed in the JMA BTD (JMA 2011; Velden et al. 2012). Not only the estimation processes but also the detailed information of the TC wind structure are somewhat different in the two BTDs. JTWC has records of radii of 35-kt winds (R35) in four quadrants (northeast, southeast, southwest, and northwest) from 2001 onward. Beginning in 2004, JTWC additionally included 50-, 64-, and 100-kt wind radii (R50, R64, and R100, respectively) in geographical quadrants in its BTD, and it replaced R35 with the 34-kt wind radii (R34). In contrast, the longest record of wind radii are of 30-kt wind radii (R30) and R50 that have been recorded in the JMA BTD since 1977. JMA simultaneously provided the longest and shortest wind radii. It also recorded the direction of the longest radius of a specified wind that can vary in eight orientations (northeast, east, southeast, south, southwest, west, northwest, and north). Therefore, this study focuses on the 6-hourly wind radii from 2004 to 2014. To make the following decompositions of wind radii more reasonable, only the storm cases with wind radii in all four quadrants in the JTWC BTD are taken into consideration. Storm records with wind radii in less than four quadrants are not utilized to derive the metrics related to the TC outer wind structure (e.g. mean wind radii, wavenumber-1 asymmetry magnitude), which is consistent with methods suggested by Demuth et al. (2006) and Knaff and Sampson (2015). During 2004–14, there are only 2, 1, and 5 (1, 6, and 2) TC records of R34_{JTWC} (R50_{JTWC}) in one, two, and three quadrants, respectively, which are negligibly small compared to the 4611 (3162) storm cases with R34_{JTWC} (R50_{JTWC}) in all four quadrants. The results shown in the following sections would not change significantly if these neglected samples were considered (figure not shown). Two types of wind radii are considered here. The first wind radius considered is the radius of gale-force winds R_{gale} , which includes R34_{JTWC} and R30_{JMA}. There are a total of 4403 simultaneous R_{gale} reports, which accounts for 95% and 72% of all wind reports in the JTWC and JMA BTDs, respectively. The second wind radius considered is the radius of storm-force winds R_{storm} , which is equivalent to R50. There are a total of 2643 simultaneous R_{storm} records, which accounts for 84% of R50_{JTWC} and 75% of R50_{JMA} reports.

The storm wind radii of either specified wind are then decomposed into their symmetric and asymmetric parts. First, the wind radii in both BTDs are arithmetically averaged to obtain their symmetric part (\bar{R}) as follows:

$$\begin{aligned} \bar{R}_{JTWC} &= \frac{1}{4}(R_{JTWC}^{NE} + R_{JTWC}^{SE} + R_{JTWC}^{SW} + R_{JTWC}^{NW}) \\ \bar{R}_{JMA} &= \frac{1}{2}(R_{JMA}^{long} + R_{JMA}^{short}), \end{aligned} \quad (1)$$

where \bar{R}_{JTWC} and \bar{R}_{JMA} are the symmetric wind radii in the JTWC and JMA BTDs, respectively. The terms R_{JTWC}^{NE} , R_{JTWC}^{SE} , R_{JTWC}^{SW} , and R_{JTWC}^{NW} refer to wind radii in the northeast, southeast, southwest, and northwest quadrants, respectively, recorded by JTWC; while R_{JMA}^{long} and R_{JMA}^{short} represent the longest and shortest wind radii, respectively, provided by JMA. The above definition is consistent with previous work (Yuan et al. 2007b; Lu et al. 2011).

A shape parameter x of the wind field can be derived from averaged R_{gale} and R_{storm} , assuming that a TC behaves like a modified Rankine vortex outside of the RMW (Liu and Chan 1999; Chan and Yip 2003; Chan and Chan 2012); that is,

$$\begin{aligned} x_{JTWC} &= \frac{\log\left(\frac{34}{50}\right)}{\log\left(\frac{R50_{JTWC}}{R34_{JTWC}}\right)} \\ x_{JMA} &= \frac{\log\left(\frac{30}{50}\right)}{\log\left(\frac{R50_{JMA}}{R30_{JMA}}\right)}, \end{aligned} \quad (2)$$

where the average radii are obtained by Eq. (1).

Second, the magnitudes of the first-order asymmetry of wind radii a are estimated as follows:

$$\begin{aligned} a_{JTWC} &= \frac{1}{2}\sqrt{(R_{JTWC}^{NE} - R_{JTWC}^{SW})^2 + (R_{JTWC}^{SE} - R_{JTWC}^{NW})^2} \\ a_{JMA} &= \frac{1}{2}(R_{JMA}^{long} - R_{JMA}^{short}). \end{aligned} \quad (3)$$

Here, a_{JTWC} and a_{JMA} refer to the wavenumber-1 asymmetry magnitudes in the JTWC and JMA BTDs, respectively. Other variables are the same as those in Eq. (1). When the wind field of the TC is perfectly symmetric, a will be zero. Otherwise, a nonzero value of a is given accompanied by the direction of the longest radius. In the JMA BTD, the orientation of the longest radius θ^{long} is directly provided as eight directions: northeast, east, southeast, south, southwest, west,

northwest, and north. In contrast, θ^{long} is estimated in the JTWC BTDC as follows:

$$\theta_{\text{JTWC}}^{\text{long}} = \arctan \left(\frac{R_{\text{JTWC}}^{\text{NE}} - R_{\text{JTWC}}^{\text{SE}} - R_{\text{JTWC}}^{\text{SW}} + R_{\text{JTWC}}^{\text{NW}}}{R_{\text{JTWC}}^{\text{NE}} + R_{\text{JTWC}}^{\text{SE}} - R_{\text{JTWC}}^{\text{SW}} - R_{\text{JTWC}}^{\text{NW}}} \right). \quad (4)$$

Then $\theta_{\text{JTWC}}^{\text{long}}$ is categorized by its value into the nearest eight directions (e.g., east is 0° , north is 90° , west is 180° , and south is 270°) in the same manner as is done for JMA.

Besides comparing the wind structures between JTWC and JMA, the Multiplatform Tropical Cyclone Surface Wind Analysis (MTCWSA) dataset (Knaff et al. 2011), which extends from 2007 to 2014, is employed as a baseline to evaluate the quality of wind radii estimates in BTDCs. The MTCWSA product provides 1-min surface wind fields on a spatial resolution of 0.1° longitude \times 0.1° latitude in a domain of 15° longitude \times 15° latitude, which are objectively estimated from multiple satellites and wind retrieval techniques. The MTCWSA uses several different satellite-based surface wind sources, including the QuikSCAT, the ASCAT, the Advanced Microwave Sounding Unit (AMSU), and several others (Knaff et al. 2011). The MTCWSA surface wind fields are bilinearly interpolated on a polar grid centered on the storm with an azimuthal resolution of 1° and then used to compute the symmetric and asymmetric parts of the TC wind structure as follows:

$$R_{\text{MTCWSA}}(\theta) = \bar{R}_{\text{MTCWSA}} + a_{\text{MTCWSA}} \cos(\theta - \theta_{\text{MTCWSA}}^{\text{long}}). \quad (5)$$

Here $R_{\text{MTCWSA}}(\theta)$ is the radius of specified winds (34 or 50 kt) in the direction θ . If the maximum wind in the direction θ is smaller than the specified wind, an undefined value will be given to $R_{\text{MTCWSA}}(\theta)$. The terms \bar{R}_{MTCWSA} , a_{MTCWSA} , and $\theta_{\text{MTCWSA}}^{\text{long}}$ refer to the averaged radius, the wavenumber-1 asymmetry magnitude, and the direction of the longest radius in the MTCWSA product, respectively. They are estimated from $R_{\text{MTCWSA}}(\theta)$ through linear regressions when there exists at least one defined $R_{\text{MTCWSA}}(\theta)$ in either of the aforementioned eight directions. Besides the wind structure, the storm intensity and central latitude are derived from the maximum surface wind and the central position in the domain for MTCWSA. In the 2007–014 period, there are 99% $R_{34\text{MTCWSA}}$ (2075 out of 2104) and 93% $R_{50\text{MTCWSA}}$ (1277 out of 1374) reports coincident with the JTWC and JMA wind radii records, respectively.

3. Potential TC-related factors influencing wind radii averages

Before comparing wind radii among datasets, it is necessary to find potential TC-related factors impacting

TC size. As mentioned in previous publications, there exist differences in TC intensity and central position between various BTDCs (Wu et al. 2006; Yeung 2006; Kamahori et al. 2006; Yu et al. 2007; Nakazawa and Hoshino 2009; Song et al. 2010; Knapp and Kruk 2010; Ren et al. 2011; Barcikowska et al. 2012; Kang and Elsner 2012). If these TC-related factors play a notable effect on wind radii, discrepancies in the former may lead to discrepancies in the latter. It is thus important to compare wind radii after removing these influences.

Figure 1 displays scatterplots of wind radii for concurrent TC records between 2004 and 2014. The relationships between wind radii and TC VMAX can be fit with quadratic functions in the two BTDCs as well as for the MTCWSA product. These shapes are similar to the fitting profile provided by Wu et al. (2015) based on the 2007–13 MTCWSA data. Although wind radii vary widely at a specified intensity, they also have their upper limits when examining them in an average sense from either dataset. Generally speaking, both R_{gale} and R_{storm} increase with increasing TC intensity and then slightly decrease after reaching a specified value. However, the intensities where the fitting curves reach their maximum values are markedly different. The term $\bar{R}_{34\text{MTCWSA}}$ ($\bar{R}_{50\text{MTCWSA}}$) has a maximum of 248 (136) km at 108 (125) kt in the fitting curves, which is consistent with that estimated by Wu et al. (2015). These intensities equate to categories 3–4 on the Saffir–Simpson hurricane wind scale. However, $\bar{R}_{34\text{JTWC}}$ and $\bar{R}_{50\text{JTWC}}$ achieve their maximums at 143 and 154 kt, respectively, which are much larger than that of $\bar{R}_{34\text{MTCWSA}}$ and $\bar{R}_{50\text{MTCWSA}}$, which equate to a category 5 on the Saffir–Simpson scale. Meanwhile, the intensities with the largest fitted values of wind radii are 103 and 110 kt for $\bar{R}_{30\text{JMA}}$ and $\bar{R}_{50\text{JMA}}$, respectively. Note that the VMAX in the BTDC is primarily estimated from satellite imagery since the termination of operational aircraft surveillance in 1987. The VMAX is derived from the current intensity (CI) number according to the Dvorak (Dvorak 1975) table and the Koba rule (Koba et al. 1990, 1991) in JTWC and JMA, respectively. The VMAX has been derived from the CI number in previous comparisons of VMAXs from different BTDCs (e.g. Nakazawa and Hoshino 2009; Knapp and Kruk 2010; Knaff et al. 2010; Barcikowska et al. 2012; Kang and Elsner 2012; Schreck et al. 2014; Choy et al. 2015). It is interesting that the aforementioned intensities for JTWC and JMA are both around a CI-number 7. This equates to the lower bound of a category 5 typhoon on the Saffir–Simpson scale. This means that the intensities with maximum wind radii are much greater in the BTDCs than those derived from MTCWSA.

Besides TC intensity, the latitude of the storm center also influences the wind radii. Early publications

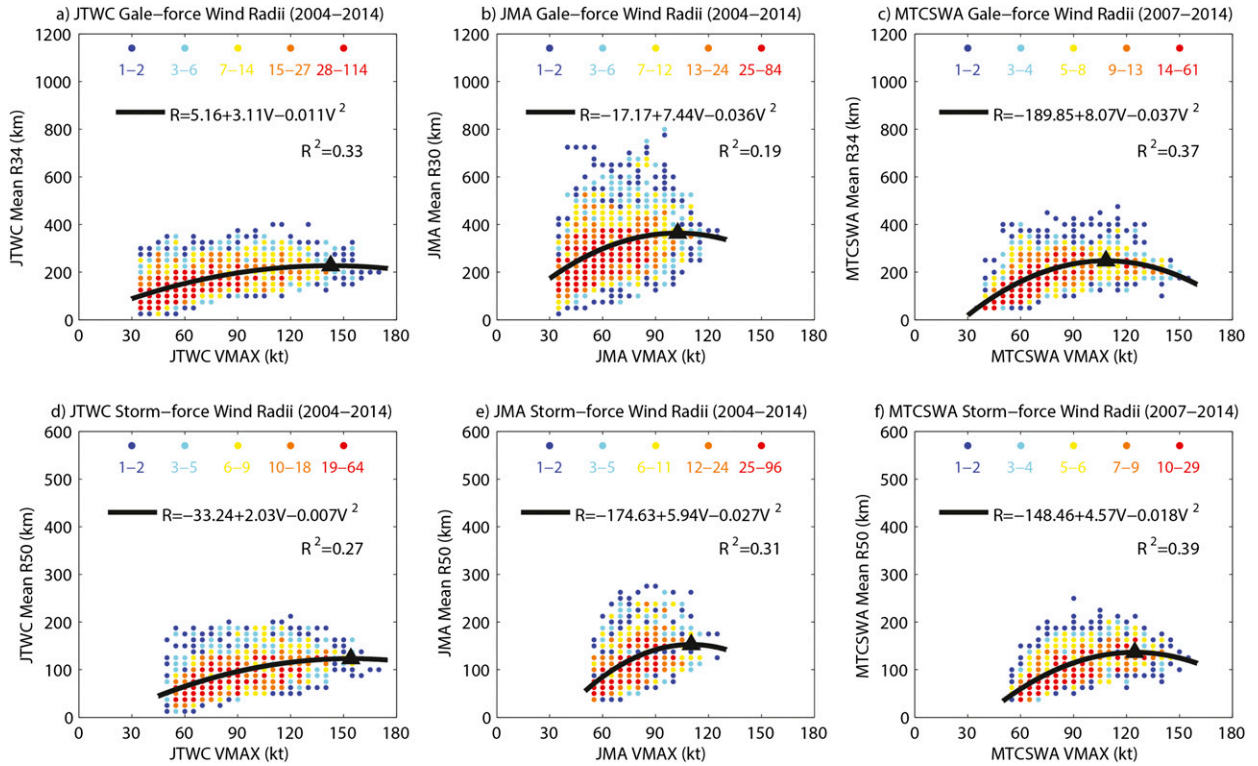


FIG. 1. Relationships between TC wind radii and maximum sustained wind speed from (a),(d) JTWC; (b),(e) JMA; and (e),(f) MTCSWA during the period from 2004 to 2014. In (a)–(c) the averaged gale-force wind radii ($\overline{R34}_{JTWC}$, $\overline{R30}_{JMA}$, and $\overline{R34}_{MTCSWA}$) are represented, while in (d)–(f) the averaged storm-force wind radii ($\overline{R50}_{JTWC}$, $\overline{R50}_{JMA}$, and $\overline{R50}_{MTCSWA}$) are shown. There are 4403, 2643, 2075, and 1277 samples in (a),(d); (b),(e); (c); and (f), respectively. The solid lines give the fitting quadratic curves, with their maximum shown by triangles.

suggested that storms tend to be larger at higher latitudes, both in observations and simulations (Yamasaki 1968; Merrill 1984; DeMaria and Pickle 1988). Using a simplified numerical simulation, Smith et al. (2011) found a nonlinear relationship between R_{gale} and the latitude at which R_{gale} increases (decreases) with the Coriolis parameter for lower (higher) latitudes. Figure 2 shows scatterplots of concurrent TCs with different wind radii and central latitudes from 2004 to 2014. The samples can also be fit with quadratic functions, although the fitting precision is a little lower than that in Fig. 1. The finding of a specified latitude for maximizing R_{gale} in Smith et al. (2011) can be applied to the BTDs and the MTCSWA as well. The fitting curves in Fig. 2 suggest that R_{gale} (R_{storm}) reaches its maximum at 29°N, 26°N, and 32°N (31°N, 27°N, and 33°N) for JTWC, JMA, and MTCSWA, respectively. This means that TC wind radii increase (decrease) with increasing latitude south (north) of a specified latitude. Similar to Fig. 1, although wind radii can vary widely at certain latitudes, there are average upper limits for R_{gale} and R_{storm} over the WNP. Note that these critical latitudes are close to the mean latitude of TC lifetime maximum intensity (LMI; Choi et al. 2016), at which TCs experience

their LMI in average. When TCs that form at lower latitudes move poleward, they will generally intensify to their LMI and then decay either because of making landfall or because of encountering cooler sea surface temperatures or larger vertical wind shears. The quadratic distribution of TC intensity in latitude is similar to that of wind radii. Further analysis indicates that wind radii are linearly related to the storm central latitude, when the influence of TC intensity is removed (figure not shown). Therefore, the quadratic relationship between wind radii and storm central latitude in Fig. 2 is greatly controlled by the meridional distribution of TC intensity.

In order to remove the influence of both storm intensity and central latitude ϕ on the variation of mean wind radius, a scaled radius R^s is calculated by dividing the observed averaged radius R by the corresponding climatological mean radius R^c as shown in Eqs. (6) and (7):

$$R^c = \alpha_0 + \alpha_1 VMAX + \alpha_2 \phi + \alpha_3 VMAX^2 + \alpha_4 VMAX \times \phi + \alpha_5 \phi^2, \quad (6)$$

$$R^s = \frac{R}{R^c}. \quad (7)$$

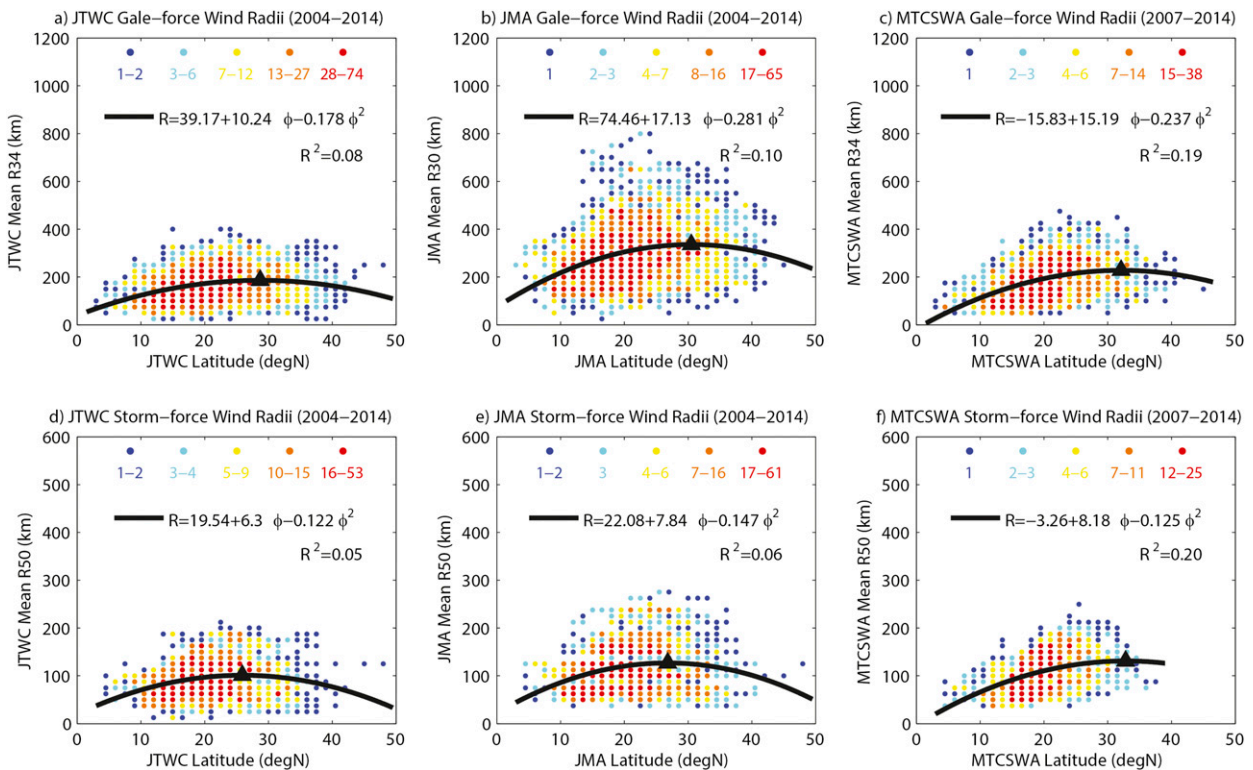


FIG. 2. As in Fig. 1, but for relationships between TC wind radii and central latitude.

This definition is similar to Knaff et al. (2014), with R^c being better estimated by considering both individual and joint effects of TC intensity and central latitude from Eq. (6). The parameters α_0 – α_5 can be estimated by least squares regression (Table 1). All regression equations are significant at the 0.001 level based on the f test. These regression equations explain much more variance than the regressions in Figs. 1 and 2. Moreover, Table 2 gives the correlation coefficients between wind radii and the two TC metrics before and after scaling. It is shown that the original mean wind radii are significantly correlated to both the TC intensity and the central latitude. By contrast, the scaled gale- and storm-force wind radii (R_{gale}^s and R_{storm}^s) are linearly independent of either the TC intensity or the central latitude.

4. Comparison of symmetric and asymmetric components of the TC wind radii

a. Symmetric part

Figure 3a displays the symmetric R_{gale} difference between JTWC and JMA for all concurrent TCs between 2004 and 2014. This figure shows that R_{gale} in one BTD can be vastly different from that displayed in another BTD. For example, when $\overline{R34}_{\text{JTWC}}$ equals 65 km, the minimum and maximum of $\overline{R30}_{\text{JMA}}$ range from 20 to

450 km, respectively. The means of $\overline{R34}_{\text{JTWC}}$ and $\overline{R30}_{\text{JMA}}$ are 166 and 295 km, which are around 50 km smaller than those estimated by Lu et al. (2011) and Yuan et al. (2007b). These differences may be caused by the different time periods analyzed in these manuscripts. Notwithstanding, there are only 178 (4% of 4403) samples with $\overline{R30}_{\text{JMA}}$ smaller than $\overline{R34}_{\text{JTWC}}$, meaning that $\overline{R30}_{\text{JMA}}$ is usually greater than $\overline{R34}_{\text{JTWC}}$. A similar result can be found by comparing two tables of 2006–08 wind radii statistics provided by Cheung et al. (2011). $\overline{R34}_{\text{JTWC}}$ and $\overline{R30}_{\text{JMA}}$ are well correlated with a correlation coefficient of 0.65, which is significant at the 0.001 level based on the Student's t test. The relationship is approximately linear with $\overline{R30}_{\text{JMA}}$ around 1.8 times $\overline{R34}_{\text{JTWC}}$.

The symmetric R_{storm} difference for all concurrent TCs during 2004–14 is displayed in Fig. 3b. The correlation coefficient between $\overline{R50}_{\text{JTWC}}$ and $\overline{R50}_{\text{JMA}}$ is 0.63, which is significant at the 0.001 level based on the Student's t test. The means of $\overline{R50}_{\text{JTWC}}$ and $\overline{R50}_{\text{JMA}}$ are 93 and 116 km, respectively. Over 75% of the samples (2011 out of 2643) have an $\overline{R50}_{\text{JMA}}$ greater than $\overline{R50}_{\text{JTWC}}$. The fitting curve in Fig. 3b also indicates that $\overline{R50}_{\text{JMA}}$ has a tendency to be larger than $\overline{R50}_{\text{JTWC}}$, with a ratio between the two mean radii of 1.26.

It is known that different averaging time periods are utilized by JTWC and JMA. Wind radii are mainly

TABLE 1. Regression coefficients and explained variances in estimating the climatological radius of a specified wind using least squares regression.

Coef	α_0	α_1	α_2	α_3	α_4	α_5	R^2
Variables		VMAX	φ	VMAX ²	VMAX \times φ	φ^2	
$\overline{R34}_{JTWC}$	-102.3	3.483	6.130	-0.011	-0.017	-0.048	0.43
$\overline{R50}_{JTWC}$	-119.4	2.300	5.595	-0.006	-0.013	-0.068	0.34
$\overline{R30}_{JMA}$	-81.0	5.207	8.678	-0.022	0.010	-0.108	0.26
$\overline{R50}_{JMA}$	-130.0	3.965	0.977	-0.018	0.033	-0.038	0.36
$\overline{R34}_{MTCSSWA}$	-275.7	6.679	8.624	-0.030	0.010	-0.101	0.53
$\overline{R50}_{MTCSSWA}$	-151.1	3.076	3.313	-0.013	0.024	-0.050	0.61

derived from satellite-retrieved surface wind fields (e.g. QuikSCAT, ASCAT). Therefore the 10-min-average wind speed can be converted into a 1-min average according to the WMO-suggested conversion table (B. Harper 2016, personal communication), in which the former is approximately 83%–95% of the latter (Harper et al. 2008). Note that a 10-min wind speed of 30 (50) kt is equivalent to a 1-min wind speed of 32–36 (53–60) kt because JTWC and JMA apply 1- and 10-min averaging for outer wind speed, respectively. Hence, $\overline{R30}_{JMA}$ should be similar to $\overline{R34}_{JTWC}$, and $\overline{R50}_{JMA}$ should be smaller than $\overline{R50}_{JTWC}$ if the wind radii estimating procedures between the two agencies were equal. However, the result is the opposite, as $\overline{R30}_{JMA}$ ($\overline{R50}_{JMA}$) is larger than $\overline{R34}_{JTWC}$ ($\overline{R50}_{JTWC}$) in most cases. Therefore, it is very likely that the differences of wind radii between JTWC and JMA result from different techniques in estimating the TC wind field rather than from the different time lengths for averaging wind speed.

The symmetric parts of R_{gale} and R_{storm} in the two BTDs are further compared with those derived from MTCSSWA between 2007 and 2014 in Figs. 3b–f. The mean of $\overline{R34}_{MTCSSWA}$ is 187 km, which is close to 1.8° found in Wu et al. (2015). It is a little larger than the 2007–14 average of $\overline{R34}_{JTWC}$ (179 km), whereas it is much lower than the 2007–14 average of $\overline{R30}_{JMA}$ (312 km). Statistically speaking, $\overline{R34}_{JTWC}$ ($\overline{R30}_{JMA}$) is approximately 0.94 (1.66) times $\overline{R34}_{MTCSSWA}$. Meanwhile, the 2007–14 means of $\overline{R50}_{MTCSSWA}$, $\overline{R50}_{JTWC}$, and $\overline{R50}_{JMA}$ are 107, 105, and 120 km, respectively. The relationship is linear, with a ratio between $\overline{R50}_{MTCSSWA}$ and $\overline{R50}_{JTWC}$ ($\overline{R50}_{JMA}$) of 0.97 (1.11). It seems that JTWC estimates the symmetric wind radii much closer to those in MTCSSWA than JMA does. Thus, the symmetric wind radii in JTWC are of higher quality than those in JMA, if the MTCSSWA product is considered as a baseline.

Estimates of both TC intensity and central latitude are significantly correlated between JTWC and JMA (Song et al. 2010; Knapp and Kruk 2010). Both of these quantities can influence wind radii to some extent. One question that naturally arises is whether the wind radii

relationship is influenced by other TC metrics. Thus, R_{JTWC}^s , R_{JMA}^s , and $R_{MTCSSWA}^s$, which exclude the effect of TC intensity and central latitude, are compared in Fig. 4. The correlation coefficients of scaled R_{gale} and R_{storm} are all significant at the 0.05 level based on the Student’s *t* test. However, they are much lower than the original (unscaled) R_{gale} and R_{storm} . This means that the linear relationships of wind radii among JTWC, JMA, and MTCSSWA are largely controlled by the relationship of TC intensity and central latitude in the three datasets. In addition, the ratios of both $\overline{R30}_{JMA}^s$ to $\overline{R34}_{JTWC}^s$ and $\overline{R50}_{JMA}^s$ to $\overline{R50}_{JTWC}^s$ are nearly 1 on average. The wind radii for JTWC are generally consistent with those for JMA after scaling. Therefore, the aforementioned statistical relationships of $\overline{R30}_{JMA} > \overline{R34}_{JTWC}$ and $\overline{R50}_{JMA} > \overline{R50}_{JTWC}$ are driven primarily by different relationships between wind radii and intensity/latitude in the two BTDs. Furthermore, the scaled mean R_{gale} and R_{storm} in two BTDs are both statistically identical to those in MTCSSWA, meaning that the wind radii in JTWC and JMA are of equal quality after scaling. Therefore, the aforementioned higher quality of original (unscaled) mean wind radii in JTWC is attributed more to a consistent statistical relationship between wind radii and the TC intensity/central latitude with MTCSSWA than anything else.

The shape parameters of concurrent TCs with both R_{gale} and R_{storm} in the two BTDs are compared from 2004

TABLE 2. Correlation coefficients between different wind radii and TC intensity/central latitude. The boldface font indicates significant values at the 0.05 level based on the Student’s *t* test.

	Intensity		Lat	
	Original	Scaled	Original	Scaled
$\overline{R34}_{JTWC}$	0.56	-0.011	0.23	-0.018
$\overline{R50}_{JTWC}$	0.50	-0.005	0.16	-0.014
$\overline{R30}_{JMA}$	0.42	0.003	0.27	-0.006
$\overline{R50}_{JMA}$	0.53	-0.003	0.19	-0.006
$\overline{R34}_{MTCSSWA}$	0.52	-0.006	0.40	-0.023
$\overline{R50}_{MTCSSWA}$	0.58	-0.010	0.43	-0.040

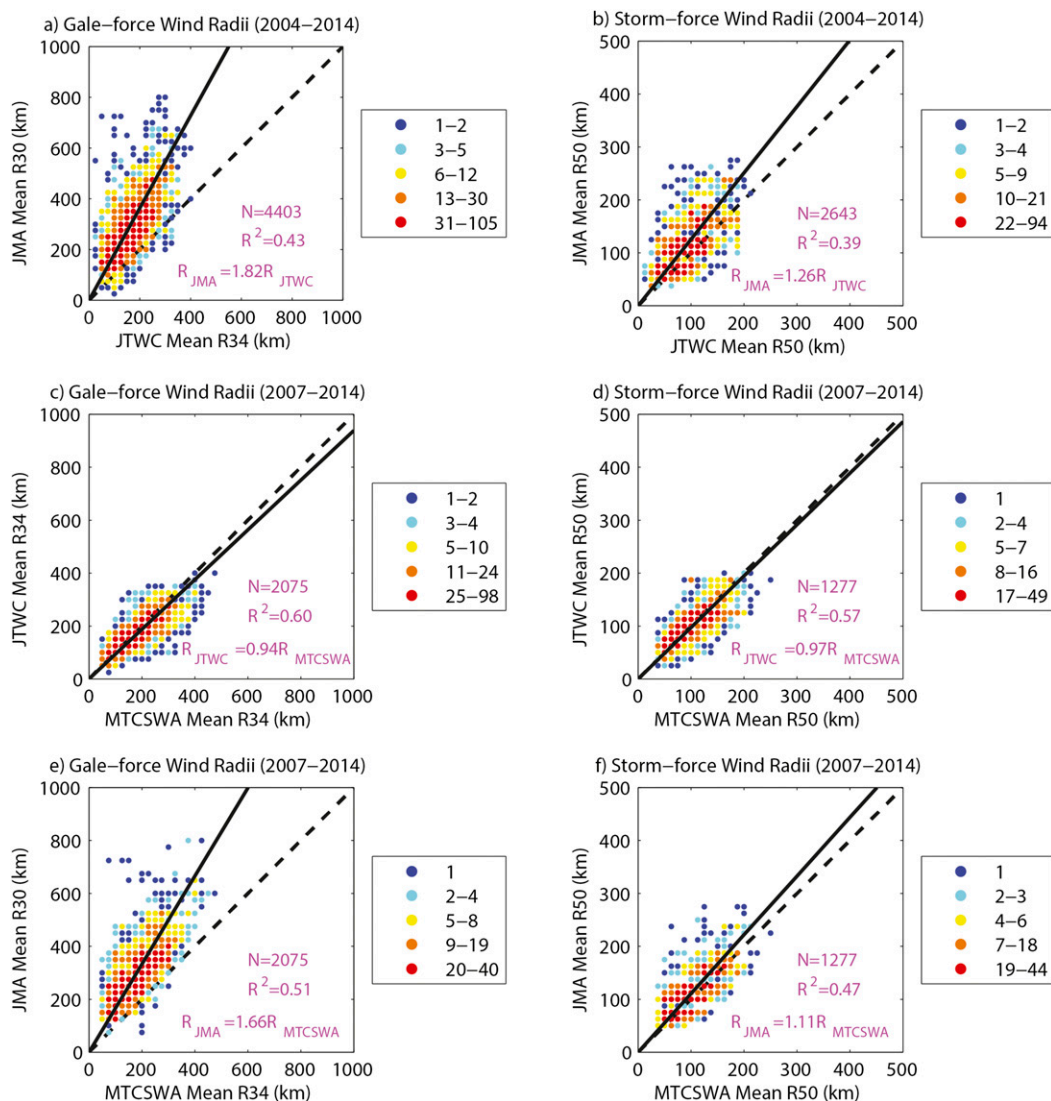


FIG. 3. Comparisons of averaged wind radii among JTWC, JMA, and MTCSSWA from 2004 to 2014. (a),(c),(e) The relationships of gale-force wind radii (i.e., $\overline{R34}_{JTWC}$ vs $\overline{R30}_{JMA}$, $\overline{R34}_{MTCSSWA}$ vs $\overline{R34}_{JTWC}$, and $\overline{R34}_{MTCSSWA}$ vs $\overline{R30}_{JMA}$, respectively). (b),(d),(f) The relationships of storm-force wind radii (i.e., $\overline{R50}_{JTWC}$ vs $\overline{R50}_{JMA}$, $\overline{R50}_{MTCSSWA}$ vs $\overline{R50}_{JTWC}$, and $\overline{R50}_{MTCSSWA}$ vs $\overline{R50}_{JMA}$, respectively). Colored circles show the frequency of occurrences at each point. Dashed black lines refer to the diagonals that define equivalent wind radii between any two datasets. Solid black lines are estimated by the total least squares. The sample size, explained variance, and linear regression slope are displayed on the plot.

to 2014 in Fig. 5a. On the one hand, the range of x_{JTWC} (0.16–1.76) is wider than that of x_{JMA} (0.22–1.09). Previous publications suggested that x generally lies between 0.4 and 0.6 (Hughes 1952; Riehl 1963; Gray and Shea 1973), indicating R_{gale} is usually 2–4 times R_{storm} . However, there are only 36% x_{JTWC} and 37% x_{JMA} in the range of 0.4–0.6. The means of x_{JTWC} and x_{JMA} are 0.55 and 0.51, respectively. The distributions of shape parameters in both BTDs are positively skewed, with only 9.4% x_{JTWC} and 2.5% x_{JMA} larger than 0.8, which means $\overline{R34}_{JTWC}$ ($\overline{R30}_{JMA}$) is approximately less than 1.6 (1.9) times

$\overline{R50}_{JTWC}$ ($\overline{R50}_{JMA}$). For larger x , there is a smaller ratio of R_{gale} to R_{storm} as well as a shorter distance between R_{gale} and R_{storm} . Moreover, 3.0% x_{JTWC} and 0.1% x_{JMA} are greater than 1, despite their nonphysical quantities in theory. Two cases with maximum shape parameters in two BTDs are given below. An x_{JTWC} of 1.76 was given to Typhoon Kujira (2009) at 0000 UTC 5 May, with $\overline{R34}_{JTWC}$ and $\overline{R50}_{JTWC}$ of 130 and 104 km, respectively. Their difference is much smaller than either wind radius, with an $\overline{R34}_{JTWC}$ to $\overline{R50}_{JTWC}$ ratio of only 1.3. Typhoon Nuri (2014) had an x_{JMA} of 1.09 at 0000 UTC

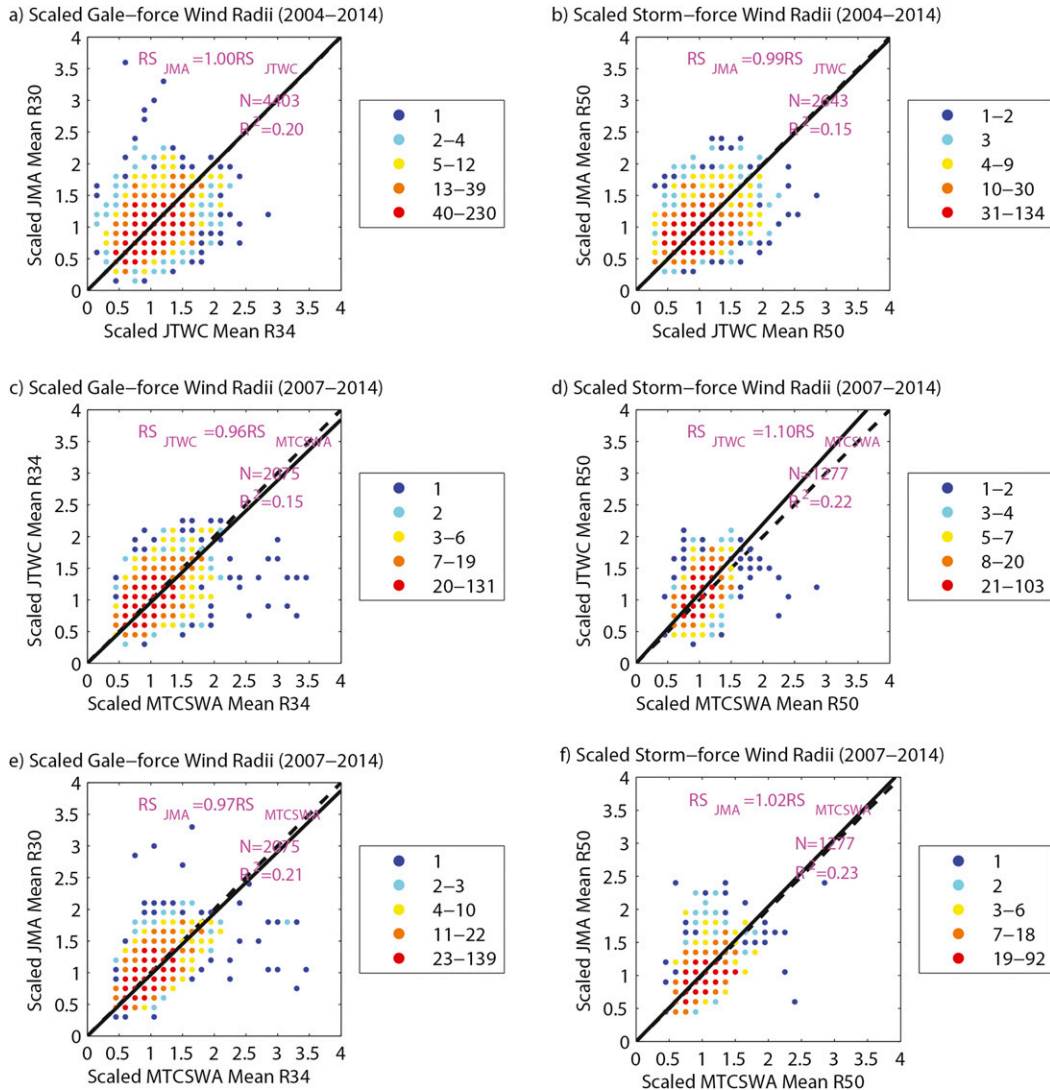


FIG. 4. As in Fig. 3, but for comparisons of scaled averaged wind radii: (a) $\overline{R34}_{JTWC}^s$ vs $\overline{R30}_{JMA}^s$, (b) $\overline{R50}_{JTWC}^s$ vs $\overline{R50}_{JMA}^s$, (c) $\overline{R34}_{MTCWSA}^s$ vs $\overline{R34}_{JTWC}^s$, (d) $\overline{R34}_{MTCWSA}^s$ vs $\overline{R30}_{JMA}^s$, (e) $\overline{R50}_{MTCWSA}^s$ vs $\overline{R50}_{JTWC}^s$, and (f) $\overline{R50}_{MTCWSA}^s$ vs $\overline{R50}_{JMA}^s$.

1 November, with $\overline{R30}_{JMA}$ and $\overline{R50}_{JMA}$ of 148 and 93 km, respectively, meaning the proportion of $\overline{R30}_{JMA}$ to $\overline{R50}_{JMA}$ is 1.6. The shape parameters between the two datasets are significantly correlated (0.21), which is significant at the 0.001 level based on the Student's *t* test. However, the low correlation also indicates a great deal of independence between the two best track datasets. The x_{JMA} is slightly smaller than x_{JTWC} (the average ratio of x_{JMA} to x_{JTWC} is 0.90). This indicates that the wind speed outside of the RMW weakens a little faster along the radial direction in the JTWC BTD. In addition, a TC is estimated to be more compact in JTWC than in JMA.

The shape parameters for the two BTDs are further compared with that for MTCWSA between 2007 and

2014 in Figs. 5b and 5c. Both x_{JTWC} and x_{JMA} are significantly correlated with x_{MTCWSA} . Generally speaking, x_{MTCWSA} is smaller (greater) than x_{JTWC} (x_{JMA}). This means that the wind structure in MTCWSA is less (more) compact than that in JTWC (JMA). The ratios of x_{JTWC} to x_{MTCWSA} and x_{JMA} to x_{MTCWSA} are approximately 1.07 and 0.86, respectively. It is thus hard to determine which BTD is better at describing the TC wind field shape.

There exists a well-known difference in the estimated TC intensity between JTWC and JMA (Wu et al. 2006; Yeung 2006; Kamahori et al. 2006; Yu et al. 2007; Nakazawa and Hoshino 2009; Song et al. 2010; Knapp and Kruk 2010; Ren et al. 2011; Barcikowska et al. 2012;

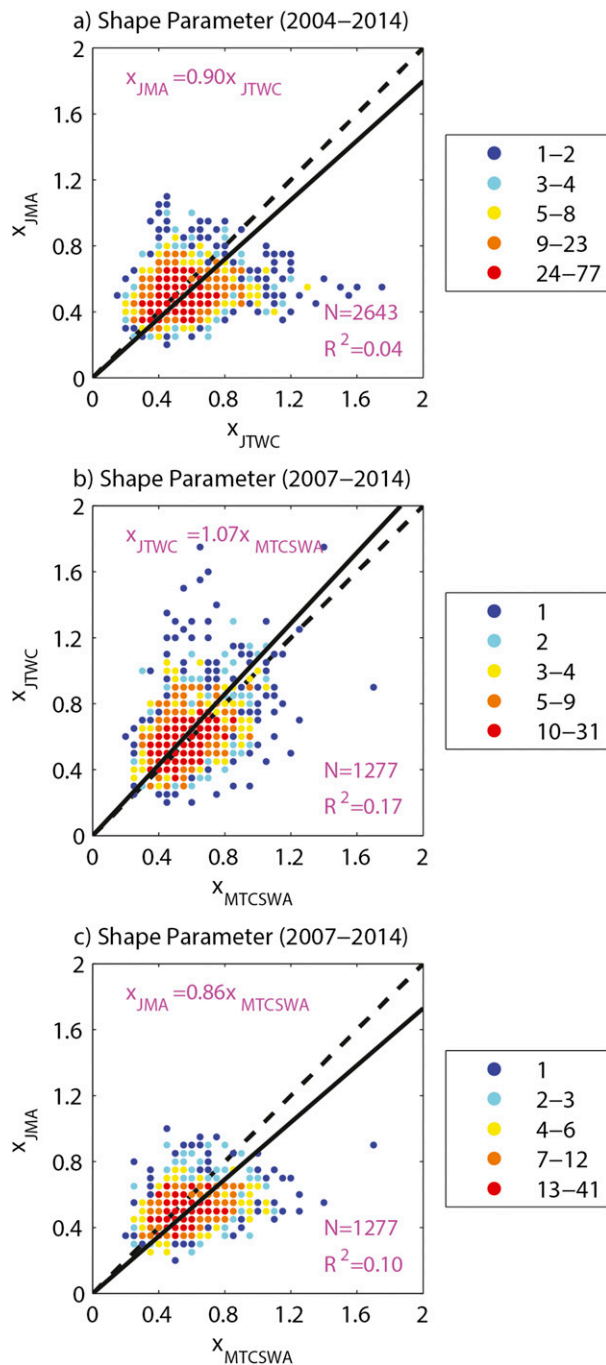


FIG. 5. As in Fig. 3, but for comparisons of storm shape parameters: (a) x_{JTWC} vs x_{JMA} , (b) x_{MTCSWA} vs x_{JTWC} , and (c) x_{MTCSWA} vs x_{JMA} .

Kang and Elsner 2012). It is also of interest to discuss whether the aforementioned discrepancy of wind radii between two BTDs (ΔR) is related to the difference of the TC intensity (ΔV). Figure 6 represents the relationships between ΔV and ΔR during 2004–14, in which ΔV (ΔR) is defined as $VMAX_{JMA}/VMAX_{JTWC}$

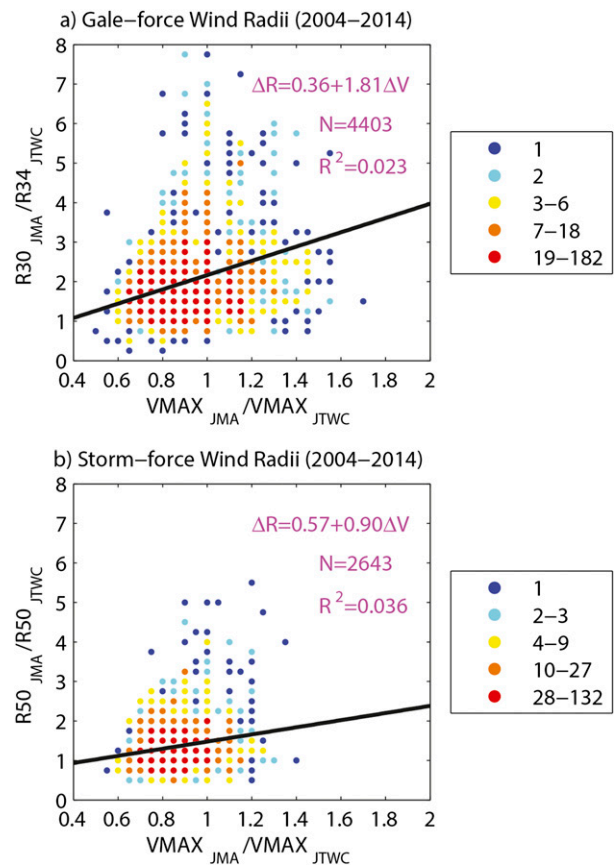


FIG. 6. Relationships between the TC intensity difference (ΔV) and the wind radius difference (ΔR) in two BTDs from 2004 to 2014. The differences are represented by the ratio of metrics in JMA to those in JTWC. The solid lines give the linear fit using least squares. The sample size, explained variance, and regression equation are displayed on the plot.

($\overline{R30_{JMA}}/\overline{R34_{JTWC}}$ and $\overline{R50_{JMA}}/\overline{R50_{JTWC}}$). When the same intensities ($\Delta V = 1$) are estimated in JTWC and JMA, $\overline{R30_{JMA}}$ ($\overline{R50_{JMA}}$) is obviously not equal to $\overline{R34_{JTWC}}$ ($\overline{R50_{JTWC}}$). Instead, ΔR is 2.16 (1.48) for gale-force (storm force) wind radii from the fitting curves in Fig. 6. This means that the averaged wind radii are inconsistent between JTWC and JMA even if there is no bias on the estimated TC intensity. However, ΔR is statistically correlated with ΔV . On average, both ratios of $R30_{JMA}$ to $R34_{JTWC}$ and $R50_{JMA}$ to $R50_{JTWC}$ increase with the increasing proportion of $VMAX_{JMA}$ to $VMAX_{JTWC}$.

b. Wavenumber-1 asymmetry magnitude

The wavenumber-1 asymmetry magnitude is another important wind field feature for determining storm intensity (Vukicevic et al. 2014). A TC wind field is often asymmetric because of the influences of its motion, surface friction, β drift, asymmetric diabatic heating,

environmental wind shear, and other factors (Uhlhorn et al. 2014). Asymmetric wind fields are frequently observed in the two BTDs as well, consistent with the statistics of $a34_{JTWC}$ and $a30_{JMA}$ between 2004 and 2014, which are usually applied as a measure of TC asymmetry. A total of 91% (4009 out of 4403) and 71% (3145 out of 4403) of all TC records are asymmetric ($a > 0$) in the JTWC and JMA BTDs, respectively. In general, JTWC represents more asymmetric storms than JMA does. Meanwhile, a similar feature can be found in the characteristics of R_{storm} . The percentage of $a50_{JTWC} > 0$ is 61% (1621 out of 2643), whereas the proportion of $a50_{JMA} > 0$ is only 23% (616 out of 2643). These results indicate that JMA estimates more symmetric storm-force wind fields rather than asymmetric ones. We discuss these asymmetries in more detail in the next few paragraphs.

Tropical cyclones are frequently estimated as symmetric in one BTD but asymmetric in another BTD. As an example of this, 28% (1107 out of 4009) $a34_{JTWC}$ and 74% (1199 out of 1621) $a50_{JTWC}$, respectively, have greater than zero values, whereas their counterparts in the JMA BTD equal zero. Taking Typhoon “Tokage” (2004) as an example, an asymmetric outer wind structure was estimated by JTWC at 1200 UTC 18 October, with $R34_{JTWC}$ ($R50_{JTWC}$) of 185, 315, 407, and 222 (130, 148, 222, and 130) km in the northeast, southeast, southwest, and northwest quadrants, respectively. By contrast, JMA assessed a symmetric storm with $R30_{JMA}$ ($R50_{JMA}$) of 741 (241) km at the same time. The percentages of asymmetric $R30_{JMA}$ and $R50_{JMA}$ recorded by JMA are 8% (243 out of 3145) and 32% (194 out of 616), respectively, when JTWC estimates a symmetric storm. As an example, JMA represented an asymmetric Typhoon “Nida” (2004) at 0000 UTC 15 May, with the longest and shortest $R30_{JMA}$ ($R50_{JMA}$) of 370 and 185 (93 and 74) km. Simultaneously, $R34_{JTWC}$ and $R50_{JTWC}$ were estimated as 250 and 111 km in the four quadrants by JTWC.

No tropical cyclone is ever going to be perfectly symmetric. A possible reason why some storms are recorded to be symmetric in BTDs is that their wavenumber-1 asymmetry magnitudes are much smaller than the average radii. Figure 7 represents the relative frequency of the normalized wavenumber-1 asymmetry magnitude a^n in MTCSWA between 2007 and 2014, when storms are recorded as symmetric or asymmetric in either BTD. Here a^n is defined by the proportion of a to the unscaled averaged wind radius, which indicates the ratio of the wavenumber-1 magnitude to the wavenumber-0 wind radius. First, relative frequency curves of $a34^n_{MTCSWA}$ for symmetric storms are separated from those for asymmetric storms in both

BTDs (Fig. 7a). The $a34^n_{MTCSWA}$ means are 0.21 and 0.25 (0.30 and 0.31) for symmetric (asymmetric) gale-force wind fields in JTWC and JMA, respectively. Asymmetric storms estimated in BTDs often have more notable wavenumber-1 asymmetries than symmetric ones. Therefore, both BTDs generally reliably describe the symmetry of the gale-force wind field. Second, relative frequency curves of $a50^n_{MTCSWA}$ are overlapped for symmetric and asymmetric storms in two BTDs (Fig. 7b). Unlike the gale-force wind field, asymmetric storms do not have greater wavenumber-1 asymmetries of the storm-force wind field than symmetric ones in either BTD. This means the symmetries of the storm-force wind field are biased and of low quality in both JTWC and JMA.

The numbers of asymmetric R_{gale} and R_{storm} reports concurrently recorded in both BTDs are 2902 (66% of 4403) and 422 (16% of 2643) during 2004–14. For these samples, the correlation coefficient between $a34_{JTWC}$ ($a50_{JTWC}$) and $a30_{JMA}$ ($a50_{JMA}$) is 0.21 (0.27), both of which are significant at the 0.001 level based on the Student’s t test. Figures 8a and 8b shows that $a30_{JMA}$ ($a50_{JMA}$) is generally larger than $a34_{JTWC}$ ($a50_{JTWC}$). This relationship is a possible result of the aforementioned relationship of $\bar{R}30_{JMA} > \bar{R}34_{JTWC}$ and $\bar{R}50_{JMA} > \bar{R}50_{JTWC}$ in an average sense. Statistically speaking, $a30_{JMA}$ and $a50_{JMA}$ are about 2.6 and 1.5 times $a34_{JTWC}$ and $a50_{JTWC}$, respectively (Figs. 8a,b). Compared with the relationships of symmetric wind radii in Fig. 3, the fitting slopes are somewhat higher for wavenumber-1 asymmetries, while the explained variances are largely reduced. This means that the relationship of the wavenumber-1 asymmetric magnitude is weaker than that of the symmetric wind radii between JTWC and JMA.

The wavenumber-1 asymmetry magnitudes of gale-force and storm-force wind fields for BTDs are also compared with those from MTCSWA in Figs. 8c–f. Although the wavenumber-1 asymmetry magnitudes in both BTDs are significantly correlated with those in MTCSWA, MTCSWA often estimates higher wavenumber-1 asymmetry magnitudes than JTWC and JMA. The statistical relationships of the gale-force (storm-force) wind asymmetry are obtained as $a34_{JTWC} = 0.28a34_{MTCSWA}$ and $a30_{JMA} = 0.79a34_{MTCSWA}$ ($a50_{JTWC} = 0.38a50_{MTCSWA}$ and $a50_{JMA} = 0.53a50_{MTCSWA}$).

Furthermore, the relationship of the normalized wavenumber-1 magnitude (a^n) is given in Fig. 9. On the one hand, the means of $a34^n_{JTWC}$ and $a50^n_{JTWC}$ are both around 0.14, while both $a30^n_{JMA}$ and $a50^n_{JMA}$ are about 0.19. Similar linear curves can be fitted to represent the a^n relationships (Figs. 9a,b). The fitting slopes are 1.28 for $a30^n_{JMA}$ to $a34^n_{JTWC}$ and 1.27 for $a50^n_{JMA}$ to $a50^n_{JTWC}$.

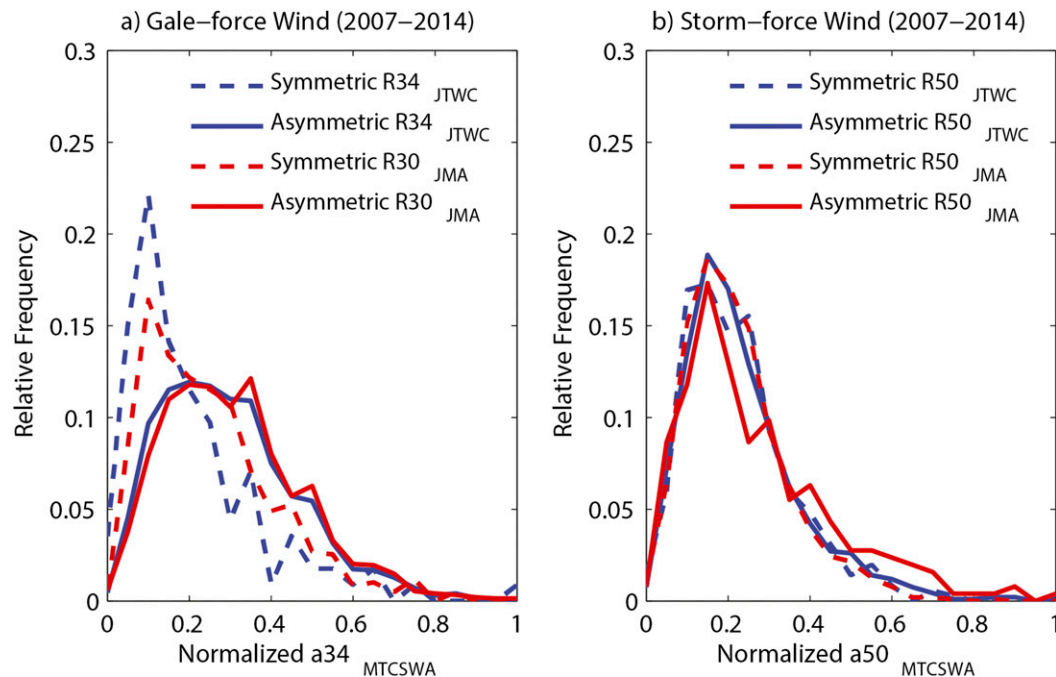


FIG. 7. Relative frequencies of normalized MTCWSA wavenumber-1 magnitudes for (a) gale-force wind radii and (b) storm-force wind radii between 2007 and 2014. Blue and red dashed (solid) lines represent symmetric (asymmetric) storms recorded in JTWC and JMA, respectively. The number of symmetric (asymmetric) $R34_{JTWC}$ and $R30_{JMA}$ are 113 and 591 (1962 and 1484) in (a), while the number of symmetric (asymmetric) $R50_{JTWC}$ and $R50_{JMA}$ are 354 and 1023 (923 and 254) in (b).

Note that although these averaged ratios are smaller than those estimated from the original nonnormalized a comparison, they are much greater than 1. This means that JMA generally estimates the storm structure with a higher wavenumber-1/wavenumber-0 ratio than JTWC does. On the other hand, both $a34_{JTWC}^n$ and $a30_{JMA}^n$ ($a50_{JTWC}^n$ and $a50_{JMA}^n$) are lower than $a34_{MTCWSA}^n$ ($a50_{MTCWSA}^n$) on average. The fitting slopes are 0.35 for $a34_{JTWC}^n$ to $a34_{MTCWSA}^n$ and 0.41 for $a50_{JTWC}^n$ to $a50_{MTCWSA}^n$. They are a little smaller than the ratio of wavenumber-1 asymmetry magnitude between JMA and MTCWSA, which are around 0.50 for $a34_{JMA}^n$ to $a34_{MTCWSA}^n$ and $a50_{JMA}^n$ to $a50_{MTCWSA}^n$. In summary, there exists a statistical relationship of $a_{MTCWSA}^n > a_{JMA}^n > a_{JTWC}^n$ and $a_{MTCWSA}^n > a_{JMA}^n > a_{JTWC}^n$, no matter what specified wind is considered.

c. Direction of the longest radius

Besides the magnitude of the wavenumber-1 asymmetry, the direction of the longest radius is another important characteristic of TC wind asymmetry. Figure 10 provides the distribution of θ^{long} for 2004–14 asymmetric storms in the JTWC and JMA BTDs. There exists a notable difference in which direction the maximum percentage is represented. For JTWC, the longest

$R34_{JTWC}$ and $R50_{JTWC}$ are both oriented most toward the east, with 43% (1714 out of 4009) of $R34_{JTWC}$ reports and 45% (735 out of 1621) of $R50_{JTWC}$ reports, respectively. The second and third most frequent directions are the northeast and north, respectively. Nearly 77% (3088 out of 4009) and 80% (1304 out of 1621) of the longest $R34_{JTWC}$ and $R50_{JTWC}$ reports, respectively, are distributed in these three directions. For JMA, the most likely orientation of the longest $R30_{JMA}$ and $R50_{JMA}$ occurs in the southeast, with 25% (796 out of 3145) of $R30_{JMA}$ and 35% (218 out of 616) of $R50_{JMA}$ records, respectively. The second and third most frequent largest directions are the east and northeast, respectively. Approximately 67% (2119 out of 3145) and 90% (553 out of 616) of storms orient their longest $R30_{JMA}$ and $R50_{JMA}$, respectively, to the southeast, east, and northeast. When only storms with a wavenumber-1 asymmetry concurrently recorded in both BTDs are considered, a similar result can be seen for the directional distribution of the longest radius (Fig. 10). This means that the longest $R34_{JTWC}$ and $R30_{JMA}$ ($R50_{JTWC}$ and $R50_{JMA}$) are not always oriented in the same direction.

During the period from 2007 to 2014, JTWC and JMA oriented their directions of the longest radius to the east,

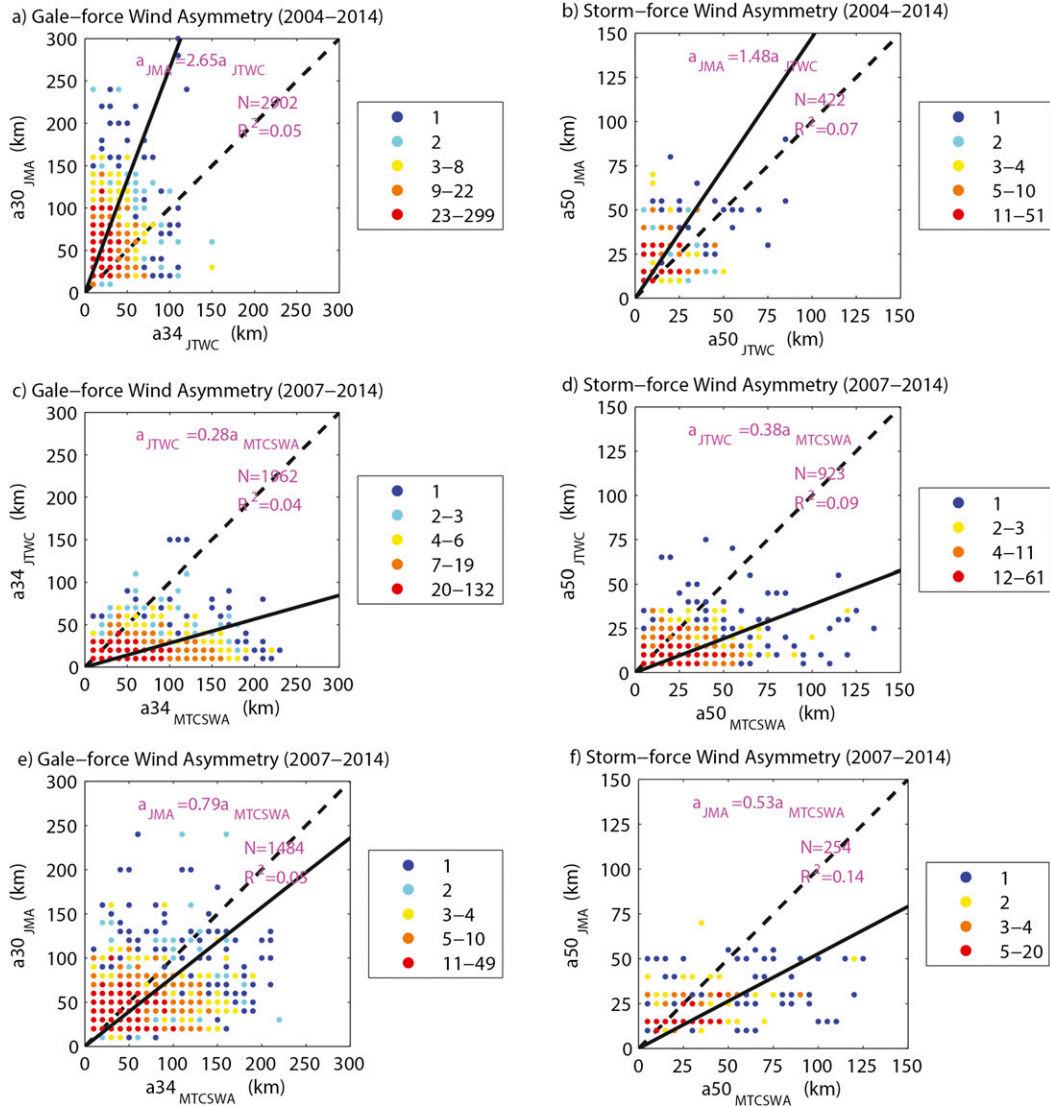


FIG. 8. As in Fig. 3, but for comparisons of original wavenumber-1 asymmetry magnitudes: (a) $a_{34_{JTWC}}$ vs $a_{30_{JMA}}$, (b) $a_{50_{JTWC}}$ vs $a_{50_{JMA}}$, (c) $a_{34_{MTCswA}}$ vs $a_{34_{JTWC}}$, (d) $a_{50_{MTCswA}}$ vs $a_{50_{JTWC}}$, (e) $a_{34_{MTCswA}}$ vs $a_{30_{JMA}}$, and (f) $a_{50_{MTCswA}}$ vs $a_{50_{JMA}}$.

northeast, north and the southeast, east, northeast, respectively (Fig. 11). The most likely orientations of the longest $R_{34_{MTCswA}}$ and $R_{50_{MTCswA}}$ both occur to the northeast. The second and third most frequent largest directions are the north and east, respectively. Note that the θ^{long} distribution in JTWC is similar to that in MTCswA (Fig. 11). However, JMA gives a somewhat different θ^{long} distribution. It appears that the θ^{long} of storms recorded in JTWC or MTCswA is rotated clockwise to that recorded in JMA.

Figure 12 further shows that only 12% (15%) of the sample size have the same directions of the longest $R_{34_{JTWC}}$ and $R_{30_{JMA}}$ ($R_{50_{JTWC}}$ and $R_{50_{JMA}}$). There

also exist 8% (7%) of records whose longest $R_{34_{JTWC}}$ and $R_{30_{JMA}}$ ($R_{50_{JTWC}}$ and $R_{50_{JMA}}$) are oriented in the opposite directions (180°). In summary, when the difference of θ^{long} is expressed as an acute angle, the θ^{long} of $R_{30_{JMA}}$ ($R_{50_{JMA}}$) has a 46% (54%) probability of rotating clockwise from that of $R_{34_{JTWC}}$ ($R_{50_{JTWC}}$). This percentage is somewhat higher than that of the θ^{long} of $R_{30_{JMA}}$ ($R_{50_{JMA}}$) shifting counterclockwise to that of $R_{34_{JTWC}}$ ($R_{50_{JTWC}}$), which accounts for about 35% (24%) of all instances. Moreover, the vector correlation coefficients defined in Hanson et al. (1992) are approximately 0.19 and 0.18 for $R_{34_{JTWC}}$ versus $R_{30_{JMA}}$ and $R_{50_{JTWC}}$ versus $R_{50_{JMA}}$, respectively. This result is

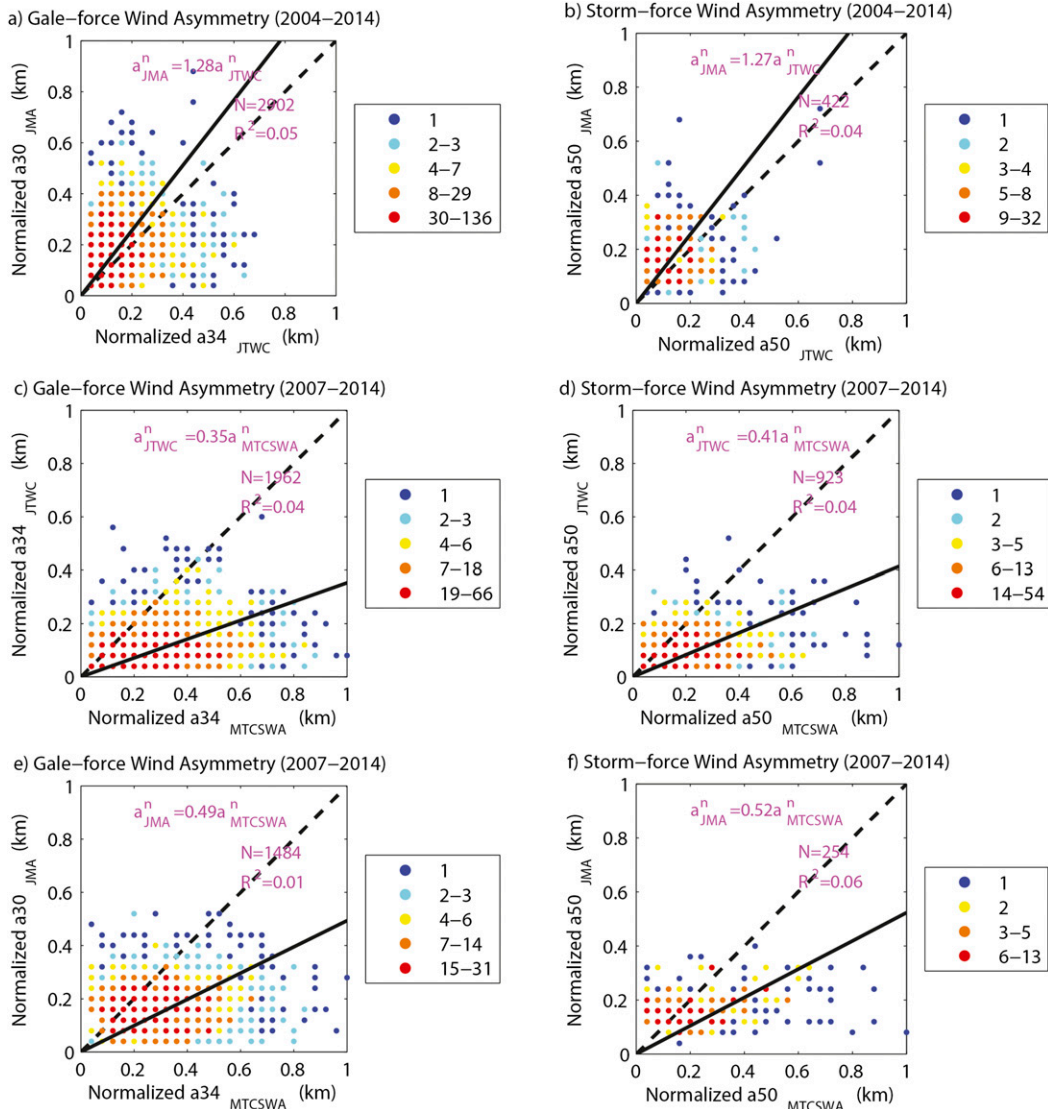


FIG. 9. As in Fig. 3, but for comparisons of normalized wavenumber-1 asymmetry magnitudes: (a) $a_{30_{JMA}}^n$ vs $a_{34_{JTWC}}^n$, (b) $a_{50_{JMA}}^n$ vs $a_{50_{JTWC}}^n$, (c) $a_{34_{MTCWSA}}^n$ vs $a_{34_{JTWC}}^n$, (d) $a_{50_{MTCWSA}}^n$ vs $a_{50_{JTWC}}^n$, (e) $a_{34_{MTCWSA}}^n$ vs $a_{30_{JMA}}^n$, and (f) $a_{50_{MTCWSA}}^n$ vs $a_{50_{JMA}}^n$.

significant at the 0.001 level based on bootstrap methods (Efron and Tibshirani 1986). On average, the θ^{long} of $R_{34_{JTWC}}$ ($R_{50_{JTWC}}$) is rotated about 18° (32°) clockwise to that of $R_{30_{JMA}}$ ($R_{50_{JMA}}$). There are also significant rotational relationships of θ^{long} for asymmetric storms concurrently recorded in JTWC (JMA) and MTCWSA, with vector correlation coefficients of 0.22 and 0.12 (0.23 and 0.17) for $R_{34_{MTCWSA}}$ versus $R_{34_{JTWC}}$ and $R_{50_{MTCWSA}}$ versus $R_{50_{JTWC}}$ ($R_{34_{MTCWSA}}$ vs $R_{30_{JMA}}$ and $R_{50_{MTCWSA}}$ vs $R_{50_{JMA}}$), respectively. Meanwhile, the θ^{long} of $R_{34_{JTWC}}$ and $R_{50_{JTWC}}$ ($R_{30_{JMA}}$ and $R_{50_{JMA}}$) are rotated about 5° and 7° (46° and 72°) counterclockwise to those of $R_{34_{MTCWSA}}$ and $R_{50_{MTCWSA}}$, respectively. This

indicates that the θ^{long} of asymmetric storms in JTWC is more consistent with that in MTCWSA.

5. Summary

In this study, the TC outer wind structures provided by two BTDs (JTWC and JMA) and the MTCWSA satellite product are compared from 2004 to 2014. Terms R_{gale} ($R_{34_{JTWC}}$, $R_{30_{JMA}}$, and $R_{34_{MTCWSA}}$) and R_{storm} ($R_{50_{JTWC}}$, $R_{50_{JMA}}$, and $R_{50_{MTCWSA}}$) are two primary metrics investigated here. The original wind radii are first decomposed into their symmetric and wavenumber-1 asymmetric components as well as the directions of their

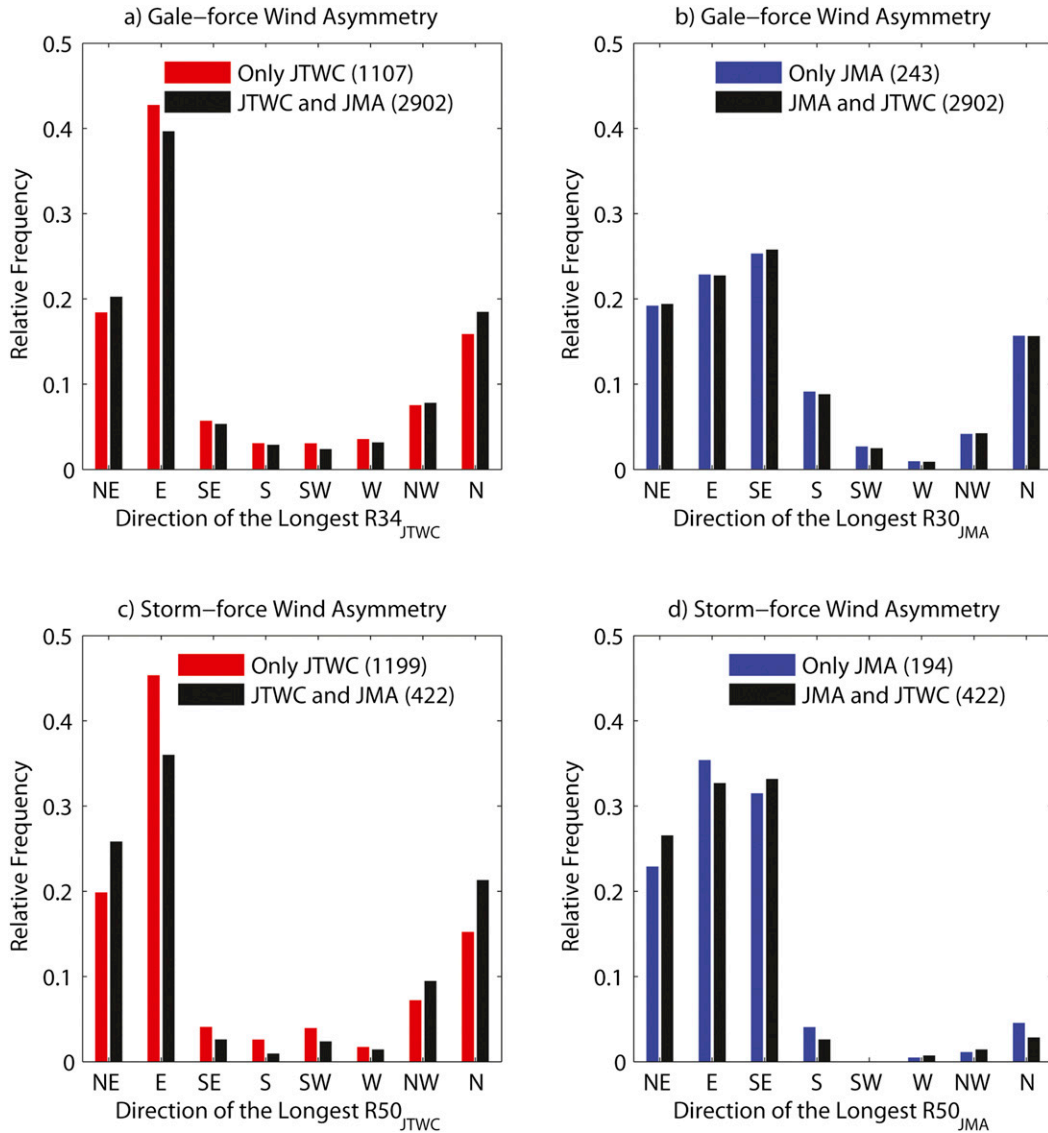


FIG. 10. Relative frequency distributions of the direction of the longest wind radius for storms with nonzero wavenumber-1 asymmetry magnitudes provided by JTWC and JMA during 2004–14. (a),(b) The gale-force and (c),(d) storm-force wind radii. Red bars in (a) and (c) display storms recorded as asymmetric only in JTWC, while blue bars in (b) and (d) show storms recorded as asymmetric only in JMA. Black bars represent TCs recorded as asymmetric concurrently by both agencies. The corresponding sample sizes are given in the legends.

longest radius. Consistent with previous publications, the symmetric part (average wind radius) is highly correlated with both TC intensity and central latitude. The relationships are furthermore fitted by quadratic functions. For both JTWC and JMA, the fitted averaged R_{gale} and R_{storm} reach their maximums at the lower bound of category 5 typhoon (CI-number 7) intensity, which is a little higher than the intensity with maximum fitted mean wind radii in MTCSWA. The fitted averages are also maximized at around 30°N. The averaged wind radii can then be statistically scaled for removing both

the individual and the joint effects of intensity and latitude on TC wind structure.

Both original and scaled mean wind radii exhibit significant linear relationships among datasets. In the comparison between two BTDs from 2004 to 2014, in an average sense the original $R30_{\text{JMA}}$ and $R50_{\text{JMA}}$ are about 1.82 and 1.26 times $R34_{\text{JTWC}}$ and $R50_{\text{JTWC}}$, respectively. This means that JMA often estimates larger TC wind radii than JTWC does. After removing the influences of intensity and latitude, $R30_{\text{JMA}}^s$ and $R34_{\text{JTWC}}^s$ are also well correlated with $R50_{\text{JMA}}^s$ and $R50_{\text{JTWC}}^s$, while the mean

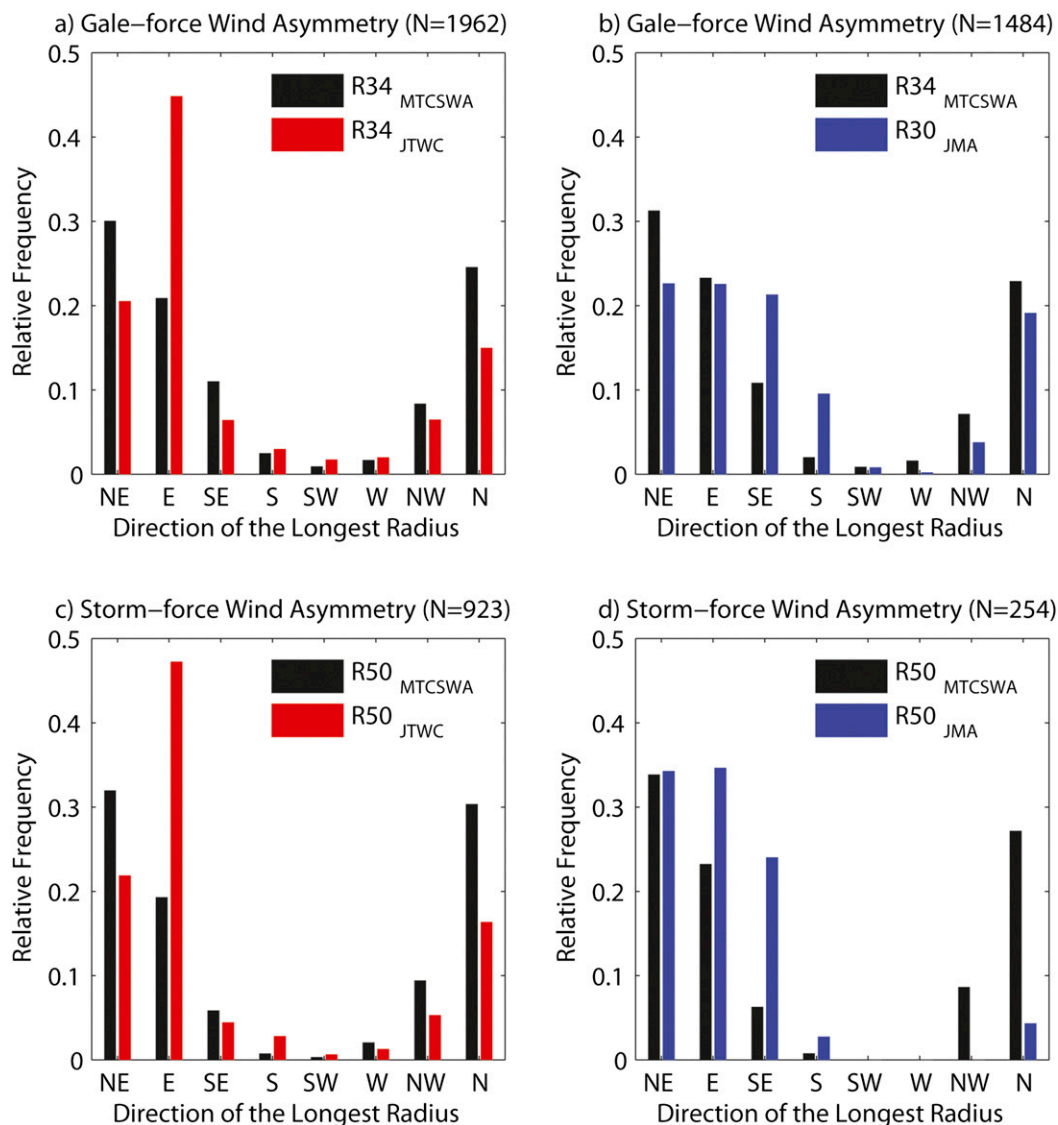


FIG. 11. Relative frequency distributions of the direction of the longest wind radius for storms with nonzero wavenumber-1 asymmetry magnitudes provided by two BTDs (JTWC and JMA) and MTCWSA from 2007 to 2014. (a),(b) The gale-force and (c),(d) storm-force wind radii. In (a) and (c) storms are recorded as asymmetric concurrently by JTWC and MTCWSA, while (b) and (d) show storms recorded as asymmetric concurrently by JMA and MTCWSA. The corresponding sample sizes are given in the figure headings.

ratios are near unity for both $\overline{R30}_{JMA}^s$ to $\overline{R34}_{JTWC}^s$ and $\overline{R50}_{JMA}^s$ to $\overline{R50}_{JTWC}^s$. The reduced correlation coefficients after scaling indicate that the relationship of original averaged wind radii is highly controlled by the assessment of intensity and latitude between JTWC and JMA. Furthermore, if a storm is considered to be a modified Rankine vortex, its shape parameter can be derived based on its averaged R_{gale} and R_{storm} . It is found that JTWC generally gives a more compact cyclone than JMA does, with a statistical relationship of $x_{JMA} = 0.90x_{JTWC}$. Taking the MTCWSA wind radii as a baseline, it is found that the unscaled averaged R_{gale} and

R_{storm} in JTWC are lower (greater) than those in MTCWSA. The mean wind radii estimated in JTWC are more consistent with those in MTCWSA, with ratios of around 0.96 (1.10) for $\overline{R34}_{JTWC}$ to $\overline{R34}_{MTCWSA}$ ($\overline{R50}_{JTWC}$ to $\overline{R50}_{MTCWSA}$).

Unlike the symmetric part, there are great differences for the wavenumber-1 asymmetry of the TC outer wind field. First, JTWC provides more asymmetric storms than JMA does, regardless of the wind radii being analyzed. Second, some storms are estimated as asymmetric by one agency but symmetric by another. A total of 3% (31%) and 66% (16%) of all samples recorded

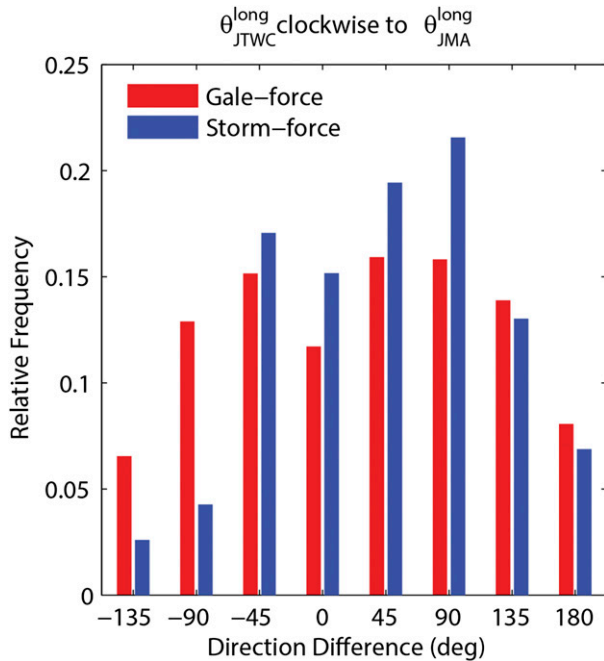


FIG. 12. Relationship of the direction of the longest wind radius (θ^{long}) for storms with nonzero wavenumber-1 asymmetry magnitudes simultaneously recorded by both JTWC and JMA from 2004 to 2014. Red and blue bars refer to the gale-force and storm-force wind radii, respectively, with sample sizes of 2902 and 422. The positive (negative) direction difference means $\theta_{\text{JTWC}}^{\text{long}}$ is rotated clockwise (counterclockwise) to $\theta_{\text{JMA}}^{\text{long}}$.

symmetric and asymmetric wind fields simultaneously in both BTDs, respectively, when R_{gale} (R_{storm}) is considered. The distributions of the relative frequencies of the MTCSSWA wavenumber-1 asymmetry magnitude are further compared between symmetric and asymmetric storms recorded in either BTD. This shows that the asymmetries of the gale-force wind field are reliable in both JTWC and JMA, since the MTCSSWA wavenumber-1 asymmetry magnitudes of symmetric storms estimated by BTDs are on average smaller than those of asymmetric ones. However, there does not exist a significant difference of the MTCSSWA storm-force wind asymmetry between symmetric and asymmetric storms in BTDs, meaning that the asymmetry of the storm-force wind field is of lower quality in both JTWC and JMA data.

Third, there exists a notable linear relationship of the wavenumber-1 asymmetry magnitude among datasets. On average, $a_{34\text{JMA}}$ and $a_{50\text{JMA}}$ are around 2.65 and 1.48 times $a_{30\text{JTWC}}$ and $a_{50\text{JTWC}}$. This is a result of the aforementioned relationship of the averaged wind radius to some extent. Meanwhile, both the mean ratios of $a_{34\text{JMA}}$ to $a_{30\text{JTWC}}$ and $a_{50\text{JMA}}$ to $a_{50\text{JTWC}}$ are still greater than one after being normalized by

corresponding averaged wind radii. By contrast, the wavenumber-1 asymmetry magnitude in MTCSSWA is much larger than those in two BTDs. The latter is about 0.3–0.6 times the latter.

For an asymmetric storm, its directions of the longest radius can be compared among two BTDs and MTCSSWA. The longest $R_{34\text{JTWC}}$ and $R_{50\text{JTWC}}$ are often oriented toward the east, northeast, and north, with the largest percentage being oriented to the east. This feature is consistent with the θ^{long} distribution in MTCSSWA. However, the orientations of the longest $R_{30\text{JMA}}$ and $R_{50\text{JMA}}$ generally occur in the southeast, east, and northeast, with the greatest proportion in the southeast. Further analysis indicates a significant rotational correlation of θ^{long} between JTWC and JMA. In an average sense, the θ^{long} of $R_{34\text{JTWC}}$ ($R_{50\text{JTWC}}$) is rotated about 18° (32°) clockwise to that of $R_{30\text{JMA}}$ ($R_{50\text{JMA}}$).

It can be seen that although wind radii are estimated by satellites in both agencies (Chu et al. 2002), the outer wind structures analyzed by each agency are indeed different. This will lead to different findings when different BTDs are used. This discrepancy is not explained simply by the different time averages utilized for wind speed estimates by the two agencies. It is very likely caused by different detailed estimating techniques. Three metrics (mean wind radius, wavenumber-1 asymmetry magnitude, and the direction of the longest radius) in JTWC are more consistent with those in MTCSSWA, which is chosen as a baseline. This means that the estimated TC wind fields are of higher quality in JTWC than in JMA, at least since 2007 when MTCSSWA data became available.

The Eighth International Workshop on Tropical Cyclones (IWTC-8; WMO 2014) recommended the WMO facilitate the standardization of TC wind radii formats among operational centers including providing more information in BTDs to verify relevant guidance products. Our results suggest that the differences of wind radii would still exist among agencies even if the same metrics related to TC outer wind structure were provided as suggested by WMO (2014). There remains an urgent need to provide a consistent and reliable process to estimate TC wind radii.

Acknowledgements. We wish to express our sincere thanks to Mr. Horoshi Ishihara at Tokyo Typhoon Center of JMA and Mr. Kenji Kishimoto at Tokyo Regional Forecast Center of JMA for their helpful comments and discussions on the JMA wind radius data. We thank Dr. Brian Strahl at JTWC for providing the information of JTWC wind radii. We also thank Dr. Bruce Harper for his suggestion on the wind conversion between different averaging times. This work

was jointly funded by the National Grand Fundamental Research 973 Program of China (2015CB452800) and the National Science Foundation of China (Grant 41575054). The second author would like to acknowledge funding support from the G. Unger Vetlesen Foundation.

REFERENCES

- Barcikowska, M., F. Feser, and H. Storch, 2012: Usability of best track data in climate statistics in the western North Pacific. *Mon. Wea. Rev.*, **140**, 2818–2830, doi:10.1175/MWR-D-11-00175.1.
- Chan, J., and C. Yip, 2003: Interannual variations of tropical cyclone size over the western North Pacific. *Geophys. Res. Lett.*, **30**, 2267, doi:10.1029/2003GL018522.
- Chan, K., and J. Chan, 2012: Size and strength of tropical cyclones as inferred from QuikSCAT data. *Mon. Wea. Rev.*, **140**, 811–824, doi:10.1175/MWR-D-10-05062.1.
- Cheung, P., C. Lam, and Y. Chan, 2011: Application of multiplatform satellite surface wind analysis in aerodrome wind forecasting during the passage of tropical cyclones. Hong Kong Observatory Reprint 981, 7 pp.
- Choi, J., Y. Cha, H. Kim, and S. Kang, 2016: Latitudinal change of tropical cyclone maximum intensity in the western North Pacific. *Adv. Meteor.*, **2016**, 5829162, doi:10.1155/2016/5829162.
- Choy, C., S. Chong, D. Kong, and E. Cayan, 2015: A discussion on the most intense tropical cyclones in the western North Pacific from 1978 to 2013. *Trop. Cyclone Res. Rev.*, **4**, 1–11, doi:10.6057/2015TCRR01.01.
- Chu, J.-H., C. R. Sampson, A. S. Levine, and E. Fukuda, 2002: The Joint Typhoon Warning Center tropical cyclone best-tracks, 1945–2000. NRL Rep. NRL/MR/7540-02-16. [Available online at http://www.usno.navy.mil/NOOC/nmfc-ph/RSS/jtwc/best_tracks/TC_bt_report.html.]
- DeMaria, M., and J. Pickle, 1988: A simplified system of equations for simulation of tropical cyclones. *J. Atmos. Sci.*, **45**, 1542–1554, doi:10.1175/1520-0469(1988)045<1542:ASSOEF>2.0.CO;2.
- Demuth, J., M. DeMaria, and J. Knaff, 2006: Improvement of Advanced Microwave Sounding Unit tropical cyclone intensity and size estimation algorithms. *J. Appl. Meteor. Climatol.*, **45**, 1573–1581, doi:10.1175/JAM2429.1.
- Dvorak, V., 1975: Tropical cyclone intensity analysis and forecasting from satellite imagery. *Mon. Wea. Rev.*, **103**, 420–430, doi:10.1175/1520-0493(1975)103<0420:TCIAAF>2.0.CO;2.
- Efron, B., and R. Tibshirani, 1986: Bootstrap methods for standard errors, confidence intervals, and other measures of statistical accuracy. *Stat. Sci.*, **1**, 54–77, doi:10.1214/ss/1177013815.
- Gray, W., and D. Shea, 1973: The hurricane's inner core region. II: Thermal stability and dynamic characteristics. *J. Atmos. Sci.*, **30**, 1565–1576, doi:10.1175/1520-0469(1973)030<1565:THICRI>2.0.CO;2.
- Hanson, B., K. Klink, K. Matsuura, S. Robeson, and C. Willmott, 1992: Vector correlation: Review, exposition, and geographic application. *Ann. Assoc. Amer. Geogr.*, **82**, 103–116, doi:10.1111/j.1467-8306.1992.tb01900.x.
- Harper, B., J. Kepert, and J. Ginger, 2008: Guidelines for converting between various wind averaging periods in tropical cyclone conditions. WMO TCP Sub-Project, October, 52 pp. [Available online at <https://www.wmo.int/pages/prog/www/tcp/Meetings/HC31/documents/Doc.3.part2.pdf>.]
- Hughes, L. A., 1952: On the low-level wind structure of tropical cyclones. *J. Meteor.*, **9**, 422–428, doi:10.1175/1520-0469(1952)009<0422:OTLLSO>2.0.CO;2.
- JMA, 2011: Operational tropical cyclone analysis by the Japan Meteorological Agency. *Int. Workshop on Satellite Analysis of Tropical Cyclones*, Honolulu, HI, National Typhoon Center, Japan Meteorological Agency, 11 pp. [Available online at <https://www.wmo.int/pages/prog/www/tcp/documents/JMAOperationalTCAnalysis.pdf>.]
- Kamahori, H., N. Yamazaki, N. Mannoji, and K. Takahashi, 2006: Variability in intense tropical cyclone days in the western North Pacific. *SOLA*, **2**, 104–107, doi:10.2151/sola.2006-027.
- Kang, N., and J. Elsner, 2012: Consensus on climate trends in western North Pacific tropical cyclones. *J. Climate*, **25**, 7564–7573, doi:10.1175/JCLI-D-11-00735.1.
- , and —, 2016: Climate mechanism for stronger typhoons in a warmer world. *J. Climate*, **29**, 1051–1057, doi:10.1175/JCLI-D-15-0585.1.
- Knaff, J., 2006: Operational guidance and skill in forecasting structure change. *Proc. Sixth WMO Int. Workshop on Tropical Cyclones (IWTC-VI)*, San Jose, Costa Rica, WMO, Topic 1.5.
- , and C. Sampson, 2015: After a decade are Atlantic tropical cyclone gale force wind radii forecasts now skillful? *Wea. Forecasting*, **30**, 702–709, doi:10.1175/WAF-D-14-00149.1.
- , —, M. DeMaria, T. Marchok, J. Gross, and C. McAdie, 2007: Statistical tropical cyclone wind radii prediction using climatology and persistence. *Wea. Forecasting*, **22**, 781–791, doi:10.1175/WAF1026.1.
- , D. Brown, J. Courtney, G. Gallina, and J. Beven II, 2010: An evaluation of Dvorak technique-based tropical cyclone intensity estimates. *Wea. Forecasting*, **25**, 1362–1379, doi:10.1175/2010WAF2222375.1.
- , M. DeMaria, D. Molenaar, C. Sampson, and M. Seybold, 2011: An automated, objective, multiple-satellite-platform tropical cyclone surface wind analysis. *J. Appl. Meteor. Climatol.*, **50**, 2149–2166, doi:10.1175/2011JAMC2673.1.
- , —, S. Longmore, and R. DeMaria, 2014: Improving tropical cyclone guidance tools by accounting for variations in size. *31st Conf. on Hurricanes and Tropical Meteorology*, San Diego, CA, Amer. Meteor. Soc., 51. [Available online at <https://ams.confex.com/ams/31Hurr/webprogram/Paper244165.html>.]
- Knapp, K., and M. Kruk, 2010: Quantifying interagency differences in tropical cyclone best-track wind speed estimates. *Mon. Wea. Rev.*, **138**, 1459–1473, doi:10.1175/2009MWR3123.1.
- , —, D. Levinson, H. Diamond, and C. Neumann, 2010: The International Best Track Archive for Climate Stewardship (IBTrACS): Unifying tropical cyclone best track data. *Bull. Amer. Meteor. Soc.*, **91**, 363–376, doi:10.1175/2009BAMS2755.1.
- Koba, H., T. Hagiwara, S. Osano, and S. Akashi, 1990: Relationship between the CI-number and central pressure and maximum wind speed in typhoon (in Japanese). *J. Meteor. Res.*, **42**, 59–67.
- , —, —, and —, 1991: Relationship between the CI-number and central pressure and maximum wind speed in typhoons. *Geophys. Mag.*, **44**, 15–25.
- Kunitzugu, M., 2012: Tropical cyclone information provided by the RSMC Tokyo Typhoon Center. *Trop. Cyclone Res. Rev.*, **1**, 51–59.
- Landsea, C., 1993: A climatology of intense (or major) Atlantic hurricanes. *Mon. Wea. Rev.*, **121**, 1703–1713, doi:10.1175/1520-0493(1993)121<1703:ACOIMA>2.0.CO;2.

- Lee, C., K. Cheung, W. Fang, and R. Elsberry, 2010: Initial maintenance of tropical cyclone size in the western North Pacific. *Mon. Wea. Rev.*, **138**, 3207–3223, doi:10.1175/2010MWR3023.1.
- Lei, X., and L. Chen, 2005: A preliminary numerical study on asymmetric wind field structure of tropical cyclones. *Chin. J. Geophys.*, **48**, 31–38, doi:10.1002/cjg2.622.
- Liu, K., and J. Chan, 1999: Size of tropical cyclones as inferred from ERS-1 and ERS-2 data. *Mon. Wea. Rev.*, **127**, 2992–3001, doi:10.1175/1520-0493(1999)127<2992:SOTCAI>2.0.CO;2.
- Lu, X., H. Yu, and X. Lei, 2011: Statistics for size and radial wind profile of tropical cyclones in the western North Pacific. *Acta Meteor. Sin.*, **25**, 104–112, doi:10.1007/s13351-011-0008-9.
- Merrill, R., 1984: A comparison of large and small tropical cyclones. *Mon. Wea. Rev.*, **112**, 1408–1418, doi:10.1175/1520-0493(1984)112<1408:ACOLAS>2.0.CO;2.
- Nakazawa, T., and S. Hoshino, 2009: Intercomparison of Dvorak parameters in the tropical cyclone datasets over the western North Pacific. *SOLA*, **5**, 33–36, doi:10.2151/sola.2009-009.
- Ren, F., J. Liang, G. Wu, W. Dong, and X. Yang, 2011: Reliability analysis of climate change of tropical cyclone activity over the western North Pacific. *J. Climate*, **24**, 5887–5898, doi:10.1175/2011JCLI3996.1.
- Riehl, H., 1963: Some relations between wind and thermal structure of steady-state hurricanes. *J. Atmos. Sci.*, **20**, 276–287, doi:10.1175/1520-0469(1963)020<0276:SRBWAT>2.0.CO;2.
- Sampson, C., P. Wittmann, and H. Tolman, 2010: Consistent tropical cyclone wind and wave forecasts for the U.S. Navy. *Wea. Forecasting*, **25**, 1293–1306, doi:10.1175/2010WAF2222376.1.
- Schreck, C., III, K. Knapp, and J. Kossin, 2014: The impact of best track discrepancies on global tropical cyclone climatologies using IBTrACS. *Mon. Wea. Rev.*, **142**, 3881–3899, doi:10.1175/MWR-D-14-00021.1.
- Smith, R., C. Schmidt, and M. Montgomery, 2011: An investigation of rotational influences on tropical-cyclone size and intensity. *Quart. J. Roy. Meteor. Soc.*, **137**, 1841–1855, doi:10.1002/qj.862.
- Song, J., Y. Wang, and L. Wu, 2010: Trend discrepancies among three best track data sets of western North Pacific tropical cyclones. *J. Geophys. Res.*, **115**, D12128, doi:10.1029/2009JD013058.
- Uhlhorn, E., B. Klotz, T. Vukicevic, P. Reasor, and R. Rogers, 2014: Observed hurricane wind speed asymmetries and relationship to motion and environmental shear. *Mon. Wea. Rev.*, **142**, 1290–1311, doi:10.1175/MWR-D-13-00249.1.
- Velden, C., and Coauthors, 2006: The Dvorak tropical cyclone intensity estimation technique: A satellite-based method that has endured for over 30 years. *Bull. Amer. Meteor. Soc.*, **87**, 1195–1210, doi:10.1175/BAMS-87-9-1195.
- , A. Burton, and K. Kuroiwa, 2012: The first International Workshop on Satellite Analysis of Tropical Cyclones: Summary of current operational methods to estimate intensity. *Trop. Cyclone Res. Rev.*, **1**, 469–481.
- Vukicevic, T., E. Uhlhorn, P. Reasor, and B. Klotz, 2014: A novel multiscale intensity metric for evaluation of tropical cyclone intensity forecasts. *J. Atmos. Sci.*, **71**, 1292–1304, doi:10.1175/JAS-D-13-0153.1.
- WMO, 2014: Recommendations addressed to WMO. IWTC-8, WMO, 4 pp. [Available online at <http://www.wmo.int/pages/prog/arep/wwrp/tmr/documents/ListofRecommendations.pdf>.]
- Wu, L., W. Tian, Q. Liu, J. Cao, and J. Knaff, 2015: Implications of the observed relationship between tropical cyclone size and intensity over the western North Pacific. *J. Climate*, **28**, 9501–9506, doi:10.1175/JCLI-D-15-0628.1.
- Wu, M., K. Yeung, and W. Chang, 2006: Trends in western North Pacific tropical cyclone intensity. *Eos, Trans. Amer. Geophys. Union*, **87**, 537–538, doi:10.1029/2006EO480001.
- Yamasaki, M., 1968: Numerical simulation of tropical cyclone development with the use of the primitive equations. *J. Meteor. Soc. Japan*, **46**, 202–214.
- Yeung, K. H., 2006: Issues related to global warming—Myths, realities and warnings. Hong Kong Observatory Reprint 647, 16 pp.
- Yu, H., C. Hu, and L. Jiang, 2007: Comparison of three tropical cyclone intensity datasets. *Acta Meteor. Sin.*, **21**, 121–128.
- Yuan, J., D. Wang, C. Liu, J. Huang, and H. Huang, 2007a: The characteristic differences of tropical cyclones forming over the western North Pacific and the South China Sea. *Acta Oceanol. Sin.*, **26**, 29–43.
- , —, Q. Wan, and C. Liu, 2007b: A 28-year climatological analysis of size parameters for Northwestern Pacific tropical cyclones. *Adv. Atmos. Sci.*, **24**, 24–34, doi:10.1007/s00376-007-0024-y.